Additive manufacturing of high-entropy alloys: Current status and challenges

Smart Materials in Manufacturing 2 (2024) 100058

Contents lists available at ScienceDirect

Smart Materials in Manufacturing

journal homepage: www.keaipublishing.com/en/journals/smart-materials-in-manufacturing

Review

Additive manufacturing of high-entropy alloys: Current status and challenges

Mehmet Cagirici [a,e], Sheng Guo [b], Jun Ding [c], Upadrasta Ramamurty [d], Pan Wang [a,*]

[a] Singapore Institute of Manufacturing Technology (SIMTech), Agency for Science, Technology and Research (A*STAR), 5 Cleantech Loop, 636732, Singapore
[b] Department of Industrial and Materials Science, Chalmers University of Technology, Gothenburg, SE-41296, Sweden
[c] Department of Materials Science and Engineering, Faculty of Engineering, National University of Singapore, Singapore, 117574, Singapore
[d] School of Mechanical and Aerospace Engineering, Nanyang Technological University, Singapore, 639798, Singapore
[e] Singapore Centre for 3D Printing, Nanyang Technological University, Singapore, 639798, Singapore

ARTICLE INFO

Keywords:
High-entropy alloys
Additive manufacturing
Alloy development
Microstructural engineering
Mechanical properties

ABSTRACT

Additive manufacturing (AM) of alloys has garnered substantial scientific and technological interest due to its applications in the manufacturing of structural components. High entropy alloys (HEAs) represent a novel class of structural materials that have received significant attention in the past two decades. AM methods such as laser powder bed fusion (LPBF) offer the capability to tailor the microstructures of alloys, facilitating the production of HEAs with tailored properties. The rapid advancements in this field necessitate an updated and comprehensive review on the design and production of HEAs specific to additive manufacturing. This review summarizes the relationships among processing parameters, microstructure, and resultant properties in AM-produced HEAs. Special attention is given to AM techniques, including powder bed fusion, directed energy deposition, and binder jet printing. This review extensively examines the effects of feedstock quality and processing parameters on the formation of metallurgical defects, as-built microstructure, mechanical behavior, and corrosion resistance of single-phase HEAs, multi-phase HEAs, and HEA matrix composites. Additionally, the applications of AM-produced HEAs, the challenges associated with their production via AM techniques, and future perspectives identified through a thorough literature survey are discussed.

1. Introduction

Over the past 30 years, additive manufacturing (AM) technologies have gained significant interest in both academia and industry for not only revolutionizing the way parts are produced, but also reducing material waste and lead time [1,2]. Pioneering studies have revealed that the materials produced by the initially proposed AM technologies, such as stereolithography (SL), selective laser sintering (SLS), and fused deposition modeling (FDM), showed some promising properties but have limited capabilities [3]. Nevertheless, advances in AM technologies have led to achieving near fully dense materials for various applications, particularly those designed for specific purposes. So far, various metallic materials with excellent mechanical properties, including steels, refractory metals and alloys, and titanium-, aluminum-, and nickel-based alloys, have been successfully produced using AM technologies [2,4]. Recently, the production of non-conventional metallic alloys, such as high entropy alloys (HEAs), has become an active area of research since these novel alloys exhibit unique and, in many cases, superior properties compared to traditional alloys. Unsurprisingly, with the hope of combining the best of both worlds, AM technologies have been employed to produce HEAs, utilizing unique advantages of AM to control the microstructure and hence to enhance material performance.

HEAs were first reported in two pioneering studies conducted by Cantor et al. and Yeh et al. in 2004 [5–7]. HEAs were initially defined as containing five or more elements in equal or near-equiatomic ratios. However, this definition was soon extended to other multi-component systems containing three and four elements without losing the characteristics of HEAs, termed medium entropy alloys (MEAs). The high mixing entropy, caused by having many constituent elements in high concentrations, stabilizes the solid solution phase against the formation of intermetallics. Typically, the solid solution phase has the face-centered cubic (FCC) [8,9], body-centered cubic (BCC) [10,11], or hexagonal close-packed (HCP) [12] structure. Depending on their compositions, HEAs could possess superior mechanical properties at

* Corresponding author.
E-mail address: wangp@simtech.a-star.edu.sg (P. Wang).

https://doi.org/10.1016/j.smmf.2024.100058
Received 28 May 2024; Received in revised form 30 August 2024; Accepted 5 September 2024
Available online 1 October 2024

various temperatures [13–18], strong resistance to oxidation [19] and corrosion [20–23], and excellent fatigue properties [24–26]. These interesting properties have attracted ever-increasing research to further explore the potential of HEAs.

Research efforts in HEAs have initially focused on forming single-phase solid solutions. Recent studies, however, have turned toward phase engineering and microstructure engineering. On the one hand, single-phase solid solutions might be destabilized under mechanical strain [27–31] or at certain temperatures [14,32–34]. On the other hand, HEAs could be strengthened by phase transformations, such as FCC to BCC [35] or FCC to HCP transformation [29,34,36], showing superior performance compared to the single-phase solid solution state. Meanwhile, the development of multi-phase HEAs has also been accelerated using computational material design, optimized materials production, and post-process heat treatments [37–43].

The first work using AM technologies, as an alternative to conventional techniques to produce HEAs, was reported in 2015 [44]. Since then, various AM techniques have been employed to produce this type of promising alloys. The processability of powders, printability of simple and complex parts, *in situ* and *ex situ* observation of microstructural evolution, and mechanical behavior of various alloy systems, such as $Al_xCoCrFeNi$, $AlCrFeMoV_x$, and TiZrNbHfTa [11,45–50], have been extensively studied to evaluate the feasibility of applying AM technologies in the alloy development and manufacturing cycles of HEAs. Directed energy deposition (DED) and powder bed fusion (PBF) AM techniques have been recently employed to illustrate the distinctive advantages on microstructural control [51–56]. These AM techniques can be used to create functionally graded alloys or particle-strengthened HEA matrix composites with desired microstructures.

Since 2015, the capability of applying AM techniques to develop HEAs with excellent characteristics has been demonstrated, which has fuelled an increase in multidisciplinary studies on HEAs. Based on the state-of-the-art literature, it has been seen that there is a necessity to employ AM techniques to manufacture various HEAs with tailorable structures and properties whilst minimizing the effort of following complicated metallurgical routes, such as alloying, melting, casting, post-processing and near-net shaping.

Consequently, numerous results on AM-ed HEAs have been reported and summarized in a few review articles [41,50,57–63]. Considering the dynamics of this rapidly developed research field, new results and, importantly, some recent excitements regarding AM-ed HEAs have not been critically reviewed. Therefore, in this comprehensive review, we summarize the state-of-the-art of AM-ed HEAs. Specifically, we review the current techniques, feedstock, microstructural evolution, and mechanical performance, and identify current challenges in the field.

2. Metal AM systems, feedstocks and processing parameters for HEAs

2.1. Metal AM systems

The American Society for Testing and Materials (ASTM) Committee F42 on Additive Manufacturing Technologies classifies AM technologies into seven categories [64]. Three out of the seven systems, i.e., powder bed fusion (PBF), directed energy deposition (DED), and binder jet printing (BJP), have been extensively employed to produce metallic components. These are schematically illustrated in Fig. 1. Among these, PBF techniques (i.e., powder bed fusion-laser beam (PBF-LB) and powder bed fusion-electron beam (PBF-EB); Fig. 1A); DED techniques (i.e., laser engineered net shaping (LENS), laser-aided additive manufacturing (LAAM), directed metal deposition (DMD), laser metal deposition (LMD) and laser deposition welding (LDW); Fig. 1B); and wire arc additive manufacturing (WAAM) were the preferred techniques for producing HEAs, as they provides an additional advantage in terms of deposition rate and microstructural design. The techniques are also grouped according to the energy source. PBF techniques are clustered as PBF-LB/laser powder bed fusion (LPBF) and PBF-EB/electron beam powder bed fusion (EPBF) where either laser beam or electron beams are employed, respectively. Simultaneously, DED techniques are grouped as directed energy deposition-laser beam (DED-LB), directed energy deposition-electron beam (DED-EB), and directed energy deposition-arc melting (DED-Arc), where either laser, electron beams or arc are used as the primary energy sources, respectively. LENS, LAAM, LMD and LDW are classified in DED-LB and WAAM is classified in DED-Arc according to the latest ASTM standard [65]. Rapid cooling and tailorable solidification behavior that are inherent to these AM techniques facilitate the microstructural control, such as grain morphology and texture. This section aims to introduce the AM technologies that could be employed to design and produce HEAs. Fig. 2 lists existing alloy systems of AM-ed HEAs, classified by different AM techniques.

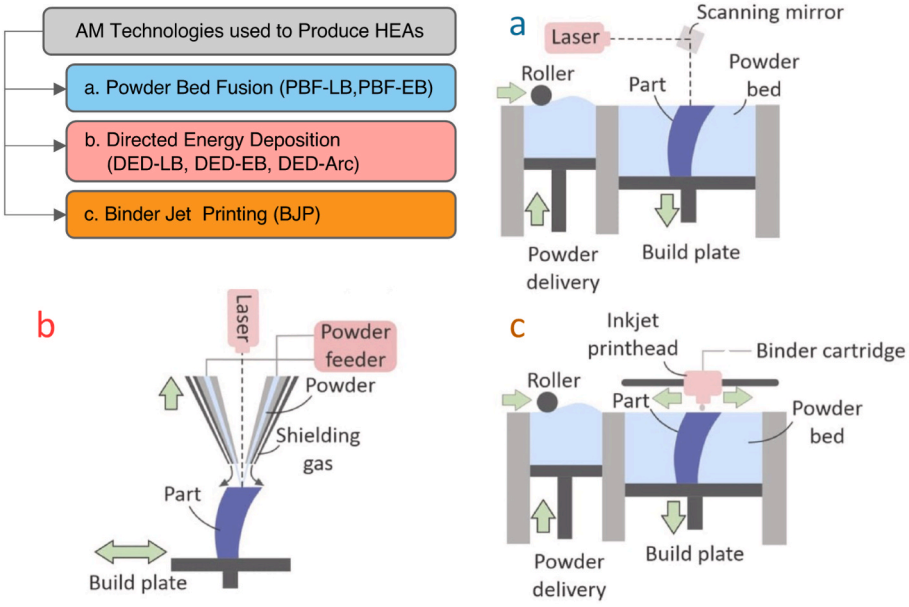

Fig. 1. Schematic illustrations of AM technologies employed to manufacture HEAs, adopted from Ref. [66]. A) Powder bed fusion (PBF), b) directed energy deposition (DED), and c) binder jet printing (BJP).

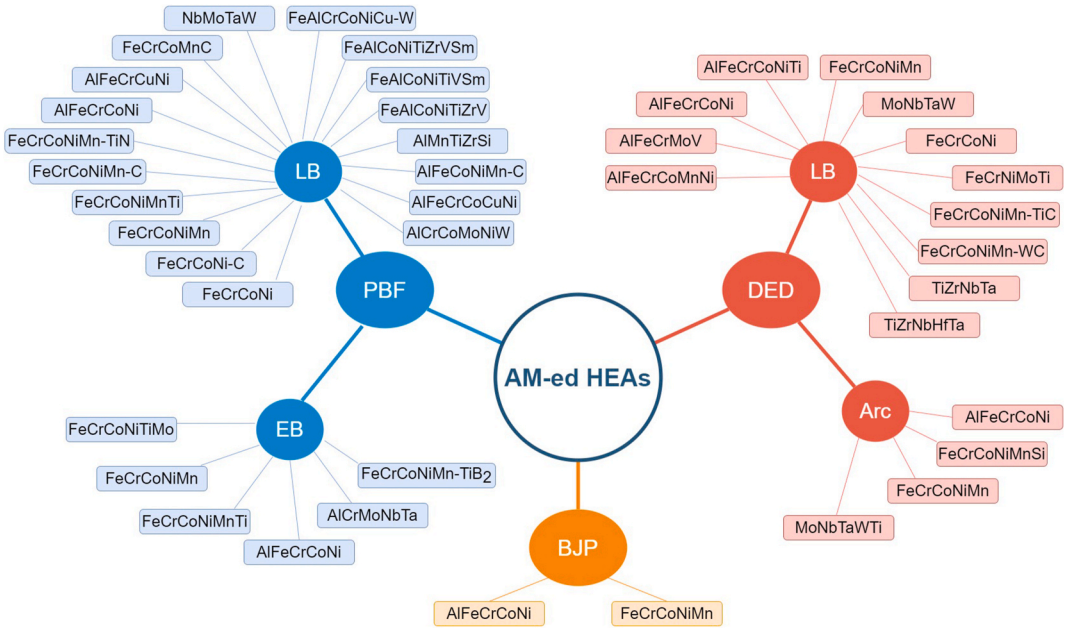

Fig. 2. Classification and schematic illustration of HEAs produced by various AM techniques.

2.1.1. *Powder-bed fusion (PBF)*

PBF techniques, including LPBF and EPBF, are widely used for producing HEAs [16,67–75] by applying focused energy [76,77]. LPBF [78] and EPBF [79–81] have become more promising methods to produce new alloys due to the following unique characteristic: The layer-by-layer fusion of the feedstock and consecutive melting/re-melting between each layer could lead to highly dense structures without the need for post-processing [82] (Fig. 1a). Although both PBF techniques offer essentially similar advantages when producing metallic parts, they differ in terms of the energy source, the printable feedstock, and the processing environment. In both techniques, a laser or electron beam is focused to liquefy the powders following pre-determined computer-aided designs. The focused energy by the laser source commonly results in a higher solidification rate than the electron beam. As a result, the microstructure of as-built parts printed by LPBF can be finer than those printed by EPBF. In addition to the reduced grain size, a higher amount of dislocations could also be observed as a result of this high solidification rate in LPBF [83]. On the other hand, EPBF might not be the better choice for achieving fine microstructure in as-built parts; it would be better to apply *in situ* heat treatments for the built parts, which brings a unique advantage when producing materials that have an intermetallic or a multi-phase structure. Detrimental intermetallics may be avoided or desired ones promoted by controlling built temperatures in EPBF [71,75,84].

2.1.2. *Directed energy deposition (DED)*

Although different types of DED systems exist, they can be classified as either powder-based or melt-based DED techniques. The main advantage of DED systems is their ability to produce compositionally graded samples along the building direction [11,85,86]. Specifically, laser-based DED techniques, such as LENS, LMD, and LAAM, have been employed to develop or to produce HEAs [49,87–95]. In all these laser-based DED techniques, laser sources heat up the powder layer or feed metal wires and increase the energy density on and around the spot, causing the feedstock to melt (Fig. 1b). The composition of the designed materials can be conveniently tuned along the building direction, generating a compositional gradient. The alloy composition is commonly manipulated using multiple feedstocks and employing elemental or pre-alloyed wires or powders brings considerable compositional freedom for achieving multi-functionality. Laminated HEAs with two or more distinct compositions can also be produced using DED [51,90].

2.1.3. *Binder jet printing (BJP)*

Sachs et al. invented the BJP technique as a three-dimensional printing technique and patented the method in 1993 [96]. The application of BJP as a metal AM technique has gained attention in recent years because of its simplicity and high productivity [97–99]. The binder and metal/ceramic materials are used as the feedstock. Metallic or ceramic powders are layered on the stage and the binder is adequately deposited to adhere the solid particles together at room temperature, as illustrated in Fig. 1c. The parts, formed by successive layer-by-layer construction of individual layers, undergo consecutive densification steps such as low- and high-temperature curing, sintering under a protective atmosphere, or hot isostatic pressing (HIP) [77,97,100]. Although BJP is a practical method for some functional applications, it has limited applicability to HEAs due to the non-fusion nature of the method. Thus, it has only been used to manufacture AlCoCrFeNi [99] and CoCrFeMnNi [101] HEAs.

2.2. *Feedstocks*

The property and quality of feedstocks have great significance on AM-ed materials since printability, microstructure, and mechanical properties are directly correlated [102,103]. The powder particles, having various powder size distribution, containing internal pores or irregularities such as satellites, can cause variations in powder flow, which may result in lack of fusion, uneven heating/cooling, porosity, cracks and high surface roughness in PBF parts [104–108]. Because of these potential issues, spherical powders are generally preferred to ensure good powder flowability and decent loos powder packing. Ensuring feedstock quality depends on various parameters, such as raw materials and feedstock synthesizing techniques. Currently, there are five synthesizing techniques for the powder feedstock, i.e., plasma rotating electrode process, water, gas, plasma, and centrifugal atomizations [109]. Gas atomization is the most promising technique for synthesizing a pre-alloyed feedstock in high quality, especially for HEAs [70]. Fig. 3 contains different feedstocks for AM. Produced from gas atomization, powders of various sizes can be utilized for LPBF [110], BJ [101] and EPBF [70] (Fig. 3a–c). Pre-alloyed HEAs powder possesses a

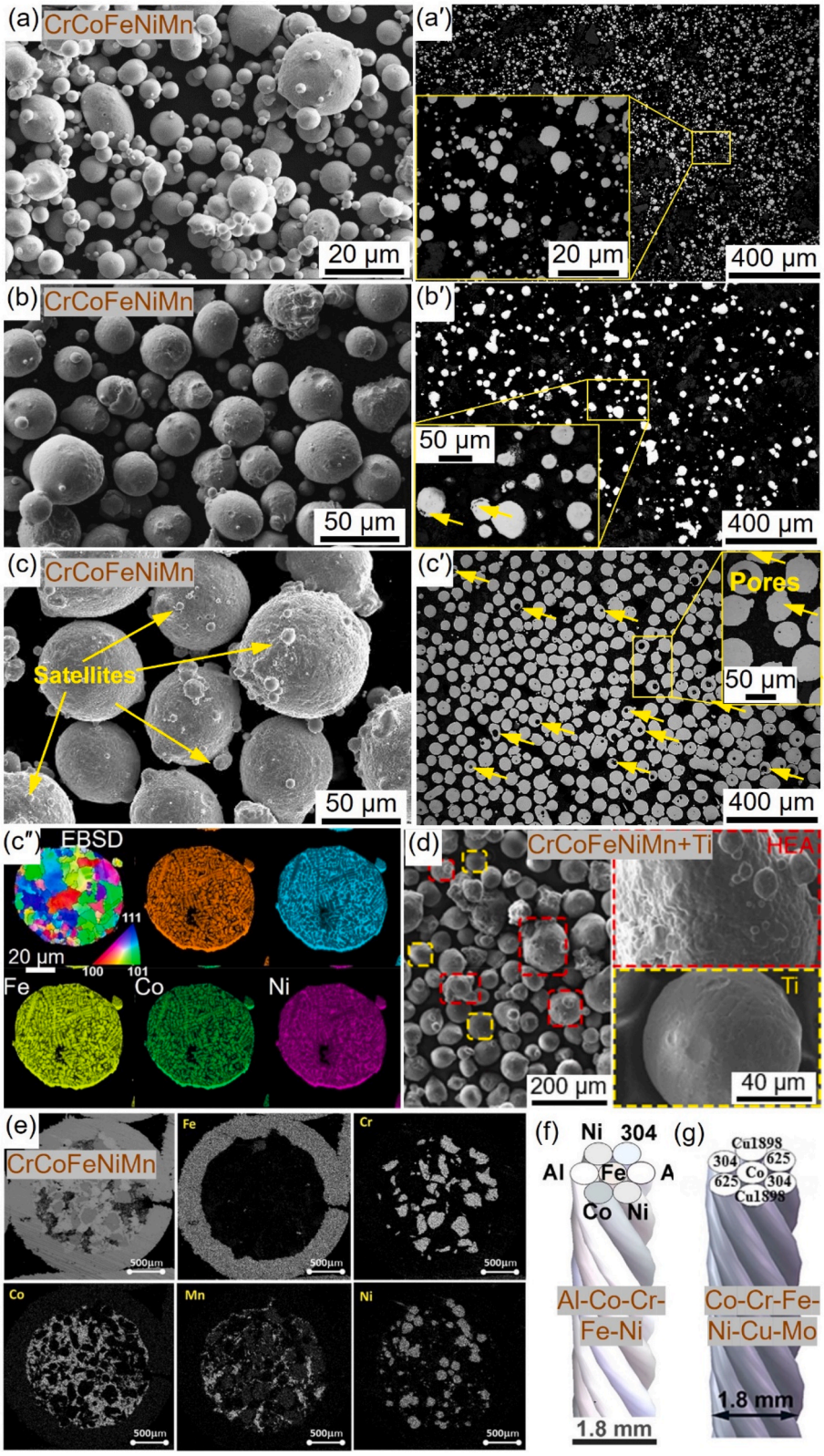

Fig. 3. Images of HEAs feedstock. (a–d) Powder with different size range for powder bed fusion and binder jetting; adapted from Refs. [70,71,101] with permission from Elsevier. (e–g) wire for wire arc additive manufacturing; adapted from Refs. [94,118,119] with permission from Elsevier.

homogeneous chemical composition (Fig. 3c″), which contributes to uniformity in the printed parts. However, the drawbacks of pre-alloying methods, including a wide particle size distribution, the creation of satellites, and the high processing cost, limit the number of alloys available in the market and their applications [111]. Additionally, entrapped gas (Fig. 3c′) can result in high porosity, necessitating further optimization efforts [70]. Recently, the mechanical mixing of elemental powders has been explored in some studies to overcome the problems of

limited range of pre-alloyed materials and the high cost of synthesizing pre-alloyed feedstocks [48,88,112,113]. The mechanical mixing can be made by applying either *in situ* or *ex situ* techniques. For most HEAs produced from mechanically mixed feedstocks, no significant issues have been reported. However, some multi-phase HEAs or intermetallic containing HEAs could not be produced successfully [71,114–116]. If the process parameters for mixed powder (Fig. 3d) are not optimized to ensure a homogeneous melting of these alloys, unmelted powder may remain.

Although powder feedstocks are preferable in the design and production of HEAs, understanding the condition of wire feedstocks is also important to obtain good wettability and printability while avoiding lack of fusion and elemental segregation. The wire feedstocks can be developed by using either commercially available, typically pre-alloyed wires [86,95], or by bundling or twisting elemental wires to obtain desired compositions [92,94,117]. For WAAM, the feedstock significantly influences the final properties. Some efforts have been made to use metal powder cored wire for non-equimolar Cantor alloys (Fig. 3e) [118] and combined cable wires for Al-Co-Cr-Fe-Ni (Fig. 3f) [94] and Co-Cr-Fe-Ni-Cu-Mo (Fig. 3g) [119]. The wire feedstocks can be applied via robotic or feed-controlled systems. By changing the wire feed rate, HEAs with a specific composition or with a compositional gradient can be produced, the latter being similar to functionally graded alloy systems [120].

2.3. Processing parameters

Processing parameters, such as process temperature, layer thickness, hatch spacing, and scanning strategy, play a significant role on feature sizes, as-built microstructures, and the resultant mechanical properties of AM-HEAs. The effect of these important parameters has been studied when producing various HEAs [86,87,113,121–127]. The principal aim when optimizing PBF and DED techniques is to achieve high densification without the existence of metallurgical defects. For example, a higher densification was achieved in the LPBF-built CoCrFeMnNi when volumetric energy density (VED) was higher than 74 J/mm^3 [122], and in the LPBF-built AlCrCuFeNi when the VED was in the range of 156 and 230 J/mm^3 [123]. These VED values have been used to gauge when various processing parameters such as scanning speed, laser power, hatch distance, and layer thickness are being optimized. For LPBF, tailoring VED values and alloy compositions can adjust the processability and the microstructure of alloys; micro- and macro-size defects might also be controlled [128–130]. Although low VED can lead to lack-of-fusion defects and reduced relative density, excessive VED may induce keyhole porosity. Additionally, VED critically impacts grain morphology (e.g., columnar vs. equiaxed), grain size distribution, and the potential formation of metastable phases in AM-ed HEAs; all of which significantly influence the final mechanical properties [131]. Interestingly, few studies have evaluated how the processing parameters for EPBF-built HEAs can be optimized. Wang et al. studied the effect of sintering temperature (900–980 °C) and holding time (20–30 min) as pre-sintering conditions of the powder bed, on EPBF of the pre-alloyed CoCrFeMnNi [70]. Other studies reported experimentally optimized processing parameters and variations in scanning strategies when producing various HEAs employing EPBF [16,67,75,132,133]. Guo et al. revealed that the scan strategy affects microstructure and mechanical properties of LPBF-built CoCrFeMnNi-(N, Si) HEAs [126]. The study showed that by employing a 45° scanning rotation, the alloy exhibits significant epitaxial growth of columnar dendrites, tolerates considerable local strain, and demonstrates lower strength, leading to higher crack densities. In contrast, the alloy utilizing a 67° scanning rotation strategy shows different structural characteristics [126]. For DED, all relevant processing parameters, such as laser power, scanning speed, beam size, and feed rate, have been explored. Parameter selection and optimization include the type of feedstock (powder or wire), the composition of the HEAs, and the target applications. Laser power of 300–3700 W, scanning speed of 100–6000 mm/min, beam size of 0.6–100 mm, and feeding rate of 2–8 g/min, have been used to fabricate various HEAs using powder feedstock in DED. For the homogeneous bulk alloys, a single parameter, for example laser power or scanning speed, was selected; for compositionally graded HEAs, a variety of parameters were applied [37,49,50,52,86,134–137]. For WAAM, wire feed speed of 5–10 m/min, arc voltage of 22–25 V, torch travel speed of 8–100 mm/min, and gas flow rate of 10–25 L/min have been explored focusing on CoCrFeMnNi and AlCoCrFeNi HEAs [94,95]. In addition to the aforementioned processing parameters, some equipment-/system-dependent parameters, such as the standoff distance of the wire feeding nozzle and torch position, may also affect the quality of produced HEAs; thus, they should also be considered for achieving high density in as-built parts.

3. Metallurgical defects

The parts produced by AM are more susceptible to metallurgical defects compared to those produced by conventional routes due to the inherent characteristics of AM techniques. Although almost all AM techniques are controlled by advanced process equipment and the manufacturing processes are pre-optimized, the formation of defects must be given special attention when producing new materials such as HEAs.

3.1. Porosity

Porosity is one of the most common metallurgical defects in metallic materials produced by AM [138–140]. Feedstock quality, beam-powder/wire interactions, and process temperature directly contribute to pore formation [105]. The powders produced by gas or plasma atomization usually contain satellites on the surface and internal porosities, which can scatter laser/electron beams and result in uneven heating/cooling parts fabrication inside the chamber. The irregularities in the heating and cooling cycles can cause widely distributed porosities in as-built parts. Furthermore, configuring AM systems to tailor the induced energy could also cause the formation of porosities: insufficient energy leads to incomplete melting while excess energy leads to the evaporation of the molten pool and gas entrapment in the melt [141]. Optimum energy density is required to liquefy high-quality feedstock without causing pore formation [139,142,143]. Real-time monitoring and control of melt pool dynamics, such as melt pool depth estimation, help maintain optimal conditions during the build process, thus minimizing porosity. Post-processing techniques like HIP, which applies high pressure and temperature to parts, effectively eliminate internal pores and improve density [140]. Additionally, adjusting manufacturing techniques, such as pulse frequency and arc current in arc additive manufacturing, can lead to finer grains and more uniform microstructures, thereby reducing porosity [144,145]. Therefore, optimizing processing parameters to obtain fully dense parts is critical for producing metallic alloys via AM [146].

3.2. Crack

Processing parameters, especially process temperature, cause cracking in various forms, such as visible cracks and interlayer cracking (delamination). These process-related cracks might be avoided or healed easily; however, material-related cracks could not be easily avoided due to the inherent compositional characteristics and microstructural features of AM-ed materials. Although HEAs were initially designed to form single-phase solid solutions, most recently developed HEAs have a multi-phase structure. The formation of various phases with differing properties leads to uneven shrinkage and localized stress concentrations within the solidifying material [147,148]. The growth stress generated between different phases might cause cracking along grain boundaries [123]. For instance, brittle phases formed in the AM-ed AlCoCrFeNi,

CoCrFeNiMn-xTi and some refractory HEAs have led to cracking [50,71]. Thermal stresses generated during continuous melting and solidification cycles can also cause visible cracks. The alloy composition plays an important role when the difference in melting points and heat capacity between constituent elements/phases is significant. Particularly, the hot cracking phenomenon are observed when exploring the effect of critical temperature range, $\Delta T = T_{liquidus}\text{-}T_{solidus}$, and kinematic viscosity on the solidification behavior of AM-ed HEAs [149]. The extensive solidification range, during which they transition from liquid to solid over a wider temperature interval, allows more time for stress buildup. Thermal stress might not be eliminated without a well-designed AM process. If the solidification between layers and along the building direction is not optimized, thermal stress or surface defects might form at the outer layers of the as-built structure. If the subsequent melting cycles do not diminish these thermal stress or surface defects, they will eventually cause the failure of as-built parts.

Some studies have focused on the cracking phenomenon in AM-ed HEAs [74,126,149–152]. These studies showed that thermal stress is responsible for crack formation, with some studies producing crack-free HEAs using LPBF. Sun et al. investigated the effect of Al addition via grain boundary engineering, which suppressed hot cracking in the LPBF-built $Al_xCoCrFeNi$ [149]. Thapliyal et al. reported that the processing window for a metastable HEA, Fe-Mn-Co-Cr-Si, could be adjusted and extended in multiple ways to control the elemental segregation and solidification structure [150]. The crack formation might also be eliminated by minimizing the critical temperature range and reducing the exposure to excessive energy density during printing. *In situ* heat treatments on each solidified layer, or post-process heat treatments at the end of printing jobs, can substantially minimize the effects of thermal stresses formed during manufacturing. Although crack formation could be mitigated via the aforementioned methodologies, some refractory HEAs are still prone to suffer from hot cracking [50]. Finding the optimal balance between minimizing cracking and achieving the exceptional strength and high-temperature properties of refractory HEAs remains a complex and active area of research [153].

4. The microstructure of AM-ed HEAs

The strong correlation between microstructure and performance of conventionally produced HEAs has been revealed using advanced material characterization techniques, such as X-ray diffraction (XRD), scanning electron microscopy (SEM), scanning transmission electron microscopy (STEM), and transmission electron microscopy (TEM). Such a correlation is also expected to exist in AM-ed HEAs, since AM techniques possess unique flexibility when it comes to tailoring the microstructure of as-built parts [50,72,154,155]. Particularly, the formation of various microstructural features and their transitions depending on the thermal gradient have been the most studied topics (Fig. 4).

The morphology of the solidified microstructure varies according to the temperature gradient and interface velocity (Fig. 4). As a result of rapid cooling achieved by PBF and DED, cellular and columnar dendritic structures are formed along the building direction [49,55,70,110,156]. The mixed grain morphology, both cellular and equiaxed, can be obtained by manipulating the scanning strategy [39,55]. Although the solidification behavior can, in principle, be tailored, the limited control over the inputs in commercialized AM equipment, including DED, LPBF and EPBF, practically restricts the ability to fullly control of the resulting microstructure.

The preferential growth of grains in alloys with cubic structures is along the <100> direction [10,70,122,123]. The strong <100> texture can be minimized or even eliminated by tailoring the scanning strategy or introducing precipitates [73,157–159]. For example, Sun et al. demonstrated the effect of scanning strategy on the microstructure of the LPBF-built CoCrFeNi [69]. Chessboard scanning was implemented to diminish the strong <011> texture, originally formed by the stripe scanning [69]. In addition to the control of grain growth by different scanning strategies, recent studies also showed that various microstructures could be achieved to meet the specific requirements for advanced applications. Hierarchical and eutectic structures, for example, were successfully generated in AM-ed HEAs [39,160–162]. Wang et al. revealed that pseudo-eutectic microstructures produced via LPBF significantly increased the yield strength of the $AlCoCrFeNi_{2.1}$ HEA [161]. Their study also showed that the change in VED during printing affected the preferential orientations of grains (Fig. 5): Finer BCC grains grew between FCC grains, where both types of grains were oriented along the <111> direction, mostly (Fig. 5i).

LPBF has proven its capability to tailor the microstructure in single- and multi-phase HEAs. However, technical limitations of EPBF and DED have yielded only limited control over the final microstructure. Thus, even though EPBF and DED bring several advantages, for example, suppressing the formation of brittle phases or forming compositionally graded structures, they are not effectively implemented to create the desired microstructures. BJP typically leads to porous structures [99,101], and the HEAs produced by BJP should in general be followed by heat treatments; they do not present directly solidified structures. The effect of AM processes on the microstructure of HEAs will be exemplified and discussed in the following sections, categorized into single-phase,

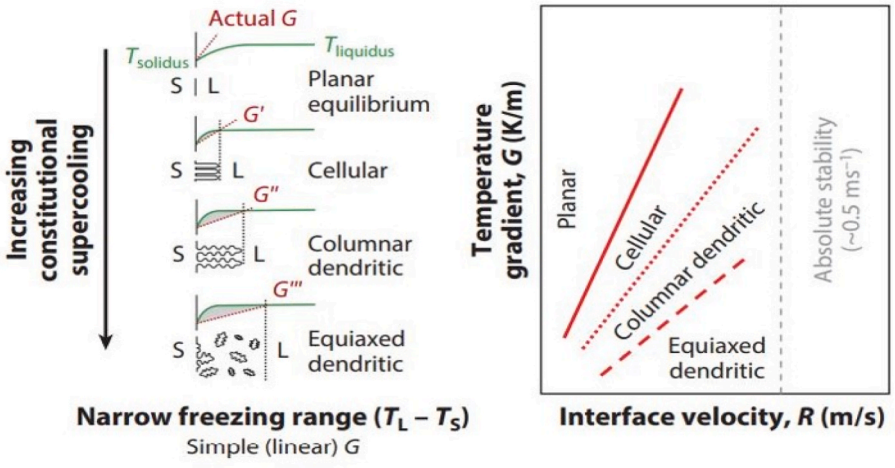

Fig. 4. Solidification behavior of metallic alloys with respect to constitutional supercooling, temperature gradients (G), and interface velocity (R); adapted from Ref. [143].

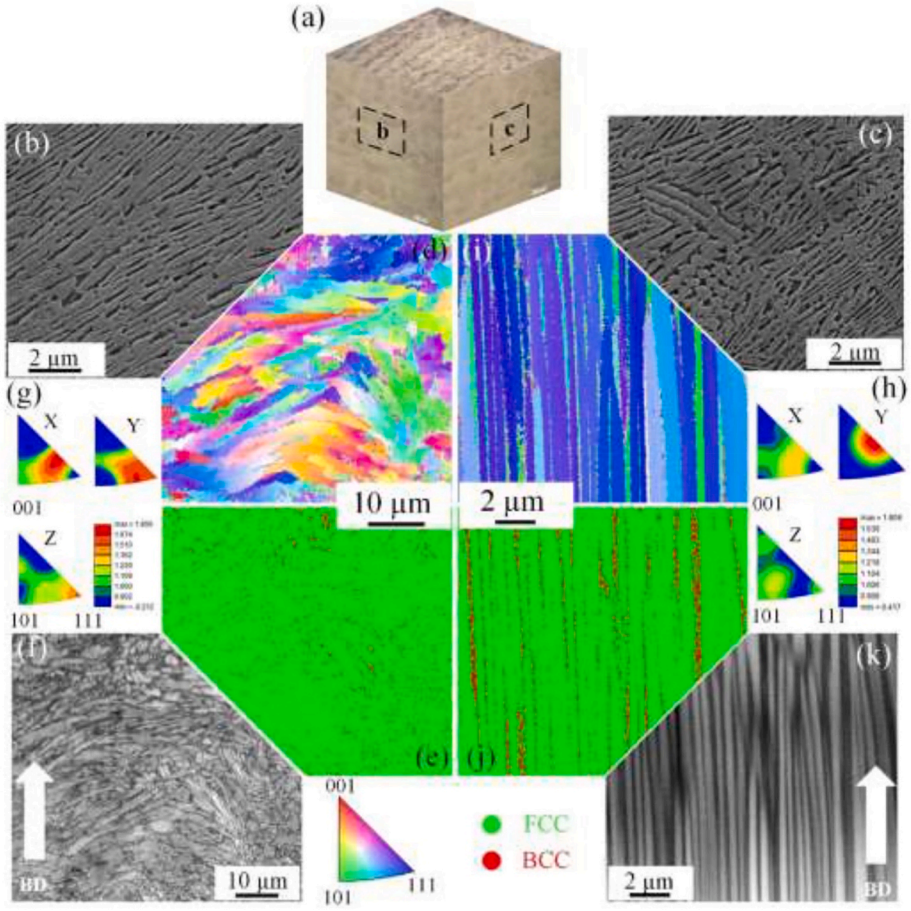

Fig. 5. Microstructural evolution of eutectic AlCoCrFeNi2.1 printed by LPBF: (a) OM images of as-built samples; (b, c) SEM images of indicated regions at the sides of the sample; EBSD images representing cross-sections along the BD under different magnification; (d, i) orientation maps (IPF-maps); (e, j) phase maps; (f, k) fore scattered diffraction images; and (g, h) pole figures with the texture index. Reprint from Ref. [161] with permission from Elsevier.

multi-phase, interstitial, and composite conditions.

4.1. *Single phase HEAs*

The formation of single-phase solid solution is frequently seen in AM-ed HEAs. CoCrFeNi systems form the basis of single-phase AM-ed HEAs, regardless of the producing techniques, mainly because CoCrFeNi is suitable for forming a solid solution with different constituents, such as Al, Cr and Mn. Furthermore, nano- or micron-sized intermetallics or precipitates, such as carbides or nitrides, can also form in this alloy system. Other than CoCrFeNi, single-phase solid solution also forms in HEA sytems such as CoCuFeNi, TiZrNbHfTa, and NbMoTaW, in as-built conditions.

4.1.1. *Single FCC solid solution*

Brif et al. produced CoCrFeNi by LPBF to show its printability back in 2015, ending up with good mechanical properties [44]. This pioneering study showed that AM-ed CoCrFeNi contains a single-phase FCC solid solution. Kenel et al. and Lin et al. further demonstrated that single-phase CoCrFeNi could be produced by different AM techniques [163,164]. Producing CoCrFeMnNi by AM has also attracted extensive research interest since 2017 [165]. Most of these works employed laser-based AM techniques, although EPBF was also used [70,166]. Haase et al. showed the successful printing of CoCrFeMnNi from elemental powders by LMD, with high homogeneity and full density [165]. Elemental segregation due to relatively slower solidification rate and high energy input during manufacturing, however, occurred in the parts produced by DED [21,167] and LAM [168,169]. For example, Melia et al. showed that Mn and Ni elements segregated in intercellular regions due to their atomic size mismatch with Co, Cr and Fe elements [21]. Chen et al. also studied the printability of CoCrFeMnNi by *in situ* alloying [116]. Although they observed elemental segregation at lower VED, successful printing without segregation was achieved at a VED of 259.3 J/mm^3 [116]. In addition to printability and segregation, they and some other researchers focused on the morphology of grains and texture development [87,116,122] in CoCrFeMnNi. Fig. 6 (a) presents the coarse columnar grains along the building direction, while nearly equiaxed grains, developed perpendicular to the building direction, were oriented close to the <100> direction (Fig. 6 b,c)[116].

Qiu et al. and Bi et al. reported the excellent mechanical performance of LAM-ed CoCrFeMnNi parts at cryogenic temperatures due to high dislocation density and deformation twinning [14,121]. Compared to the as-cast material, the dislocation density of LAM-ed alloy increased by more than 100 % depending on the crystal orientation [14]. Li et al. showed the presence of nano-twins in LPBF-built CoCrFeMnNi at a true strain of $\leq$3.7 %, which were not observed in as-cast and deformed alloys [122]. The microstructural evolution of the LPBF-built CoCrFeMnNi is presented in Fig. 7, where dislocation pile-ups, precipitates, stacking faults, and nano-twins can be seen. The σ precipitates occurred with subsequent heating cycles (Fig. 7 b,c).

Xiang et al. observed coarse columnar grains at the bottom of DED-ed CoCrFeMnNi parts due to subsequent melting of the layers, while relatively fine columnar and equiaxed grains were seen along the building direction. This change in microstructure was correlated to constitutional undercooling, where overlapping layers in thin wall formation caused melting of previous layers, leading to equiaxed grains at the top of the

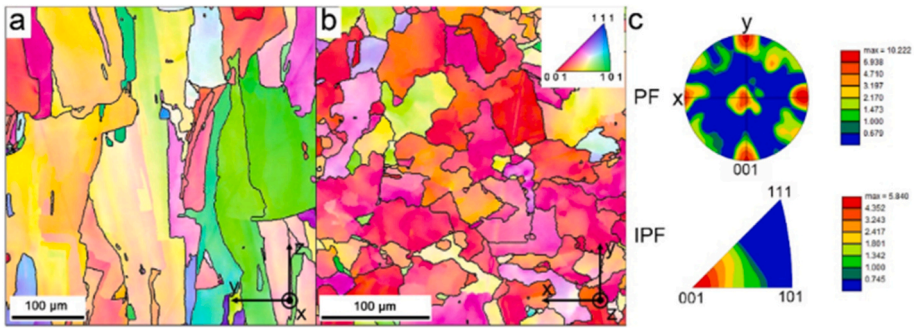

Fig. 6. (a) The perpendicular plane and (b) the horizontal plane of the LPBF-built CoCrFeMnNi and (c) PF and IPF of the horizontal plane. Reprint from Ref. [116] with permission from Elsevier.

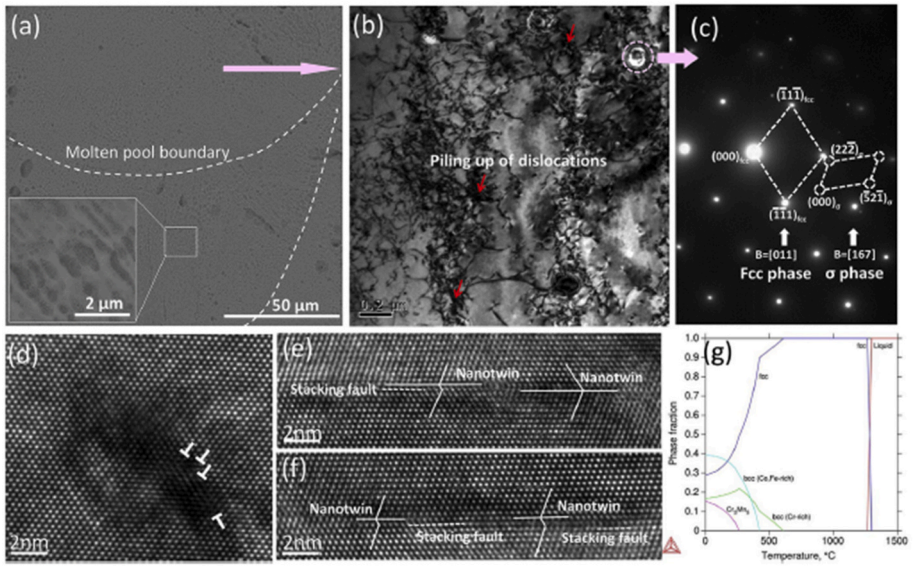

Fig. 7. The microstructure of the LPBF-built CoCrFeMnNi. (a) SEM image showing the laser molten pool boundary and sub-micron cellular grains; (b) TEM bright-field image showing the high density of dislocation pile-ups and dislocation network; (c) SAED pattern showing the primary FCC phase and the tetragonal σ precipitate; (d) HRTEM showing dislocations; (e, f) HRTEM showing the nano-twins and stacking faults; (g) calculated equilibrium phase fractions for CoCrFeMnNi. Reprint from Ref. [122] with permission from Elsevier.

molten pool being melted and columnar grains growing epitaxially, but increased laser power and deposition height result in heat accumulation and columnar-to-equiaxed structure transitions [87]. Zhu et al. showed how the formation of columnar grains affected the strengthening mechanism of LPBF-built CoCrFeMnNi [110], where cellular grains along the building direction did not contribute much to the strengthening, compared to that from dislocation hardening [110]. In addition to the detailed investigation of cellular formation on LPBF-built HEAs, Wang et al. investigated the cellular structure formation on CoCrFeMnNi HEA manufactured via EPBF (Fig. 8) [70]. It was reported that the cellular structure size of EPBF-built HEA lies between as-cast and LPBF-built parts because of the relatively faster cooling rate of EPBF than casting (10–20K/s) but slower than LPBF (up to 10^7 K/s) [70]. Although the faster cooling rate contributed to reducing the size of cellular structures, Wang et al. noted that *in situ* heat treatment during printing led to comparable mechanical properties of EPBF-built materials with their as-cast counterparts [70]. In brief, various AM techniques were proven as suitable to manufacture CoCrFeMnNi HEA; however, LPBF and EPBF techniques might be concluded as providing more flexibility to control the microstructure of AM-ed parts while eliminating the elemental segregation. Designing either process considering molten pool kinetics and solidification dynamics might be helpful to fabricate CoCrFeMnNi alloys with varying microstructure as well as mechanical properties. Changes in grain morphology, size, and texture will further result in achieving the desired characteristics for a single phase HEAs, mostly valid for the ones having FCC structure, with respect to applications. Joseph et al. investigated the microstructural evolution in Al0.3CoCrFeNi HEAs after HIP. [170]. The HIP treatment at 1100 °C for 2 hours maintained the strong <001> texture while eliminating second-phase grain boundary phases and segregation, resulting in chemical homogenization

4.1.2. *Single BCC solid solution*

The effect of adding Al in CoCrFeNi has been studied to explore the formation mechanism of BCC solid solution for many years [8,10,16,47,49,68,89,133,171,172]. Single-phase BCC solid solution in the Al_x-CoCrFeNi system was first produced by Joseph et al. [47]. AM-ed Al_x-CoCrFeNi HEAs showed a strong <001> texture due to the existence of columnar grains along the fast heat transfer direction [47,68]. Columnar, cellular, or a mixture of both structures were observed in the produced Al_xCoCrFeNi HEA parts by DED, LPBF, and EPBF, regardless of the alloy compositions [49,87,110,173].

Gwalani et al. showed that V has good solubility in the AlCrFeMo HEA, and did not cause any structural change in the BCC solid solution; however, it decreased the lattice parameter and strengthened the <001> diffraction [11]. Dobbelstein et al. used LMD to synthesize

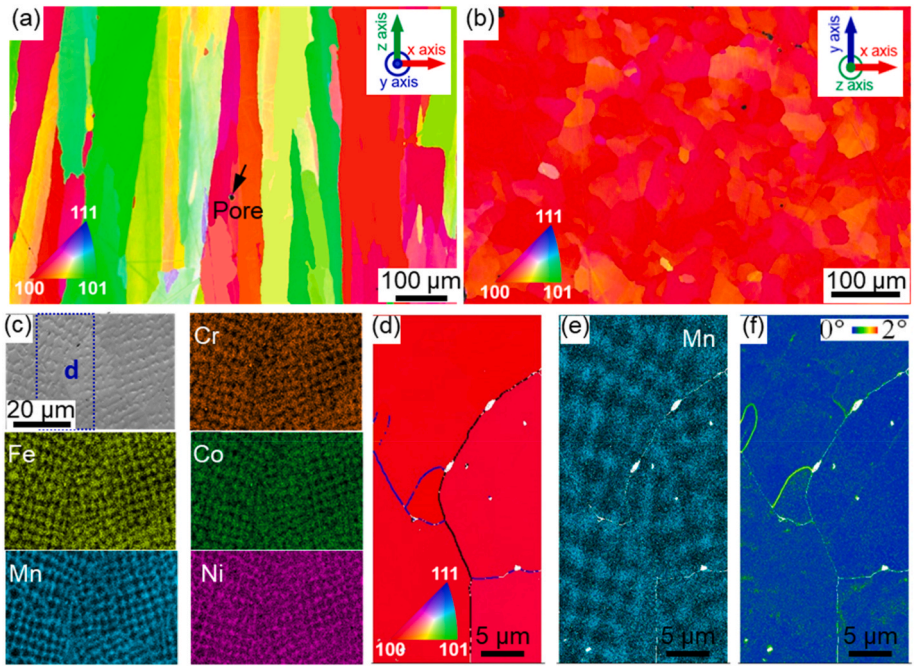

Fig. 8. EBSD-IPF maps on the (a) XZ and (b) XY plane of the EPBF-built CoCrFeMnNi; (c) SEM image and the corresponding elemental distributions on the XY plane; (d) EBSD-IPF map on the enlarged zone showing the grain boundaries; (e) corresponding Mn element distribution; and (f) KAM image of the region highlighted in (c). Adapted from Ref. [70] with permission from Elsevier.

single-phase BCC structured TiZrNbHfTa HEA from mixed powder and revealed that compositional homogeneity was achieved when the height of the printed part was above 2 mm [88]. Ishimato et al. produced TiNbTaZrMo-based BioHEA via LPBF, aiming to improve yield strength and ductility [157]. They observed suppressed elemental segregation, together with bimodal grain size distribution within the melt pool (Fig. 9) [157]. Zhang et al. produced single-phase BCC structured NbMoTaW HEA by LPBF, with exceptionally fine grains and better mechanical properties than as-cast counterparts [174].

Zhang et al. studied the microstructure of the AlCoCuFeNi HEA produced by LPBF [68]. Fig. 10 illustrates the textural development of the alloy along XY and XZ planes. Because of the designed scanning strategy (a 90° rotation was made at each new layer), equiaxed grains were formed along the XY plane (Fig. 10a). Along the XZ plane, epitaxially grown BCC_B2 grains were seen, with strong <001> texture (Fig. 10 b-d).

4.1.3. *Interstitial high entropy alloys*

Introducing interstitial elements into HEAs has proven to be a promising method to improve the mechanical performance of the alloys. A small addition of interstitial elements could promote the formation of, for example, carbides and nanosized precipitates, as well as activate new

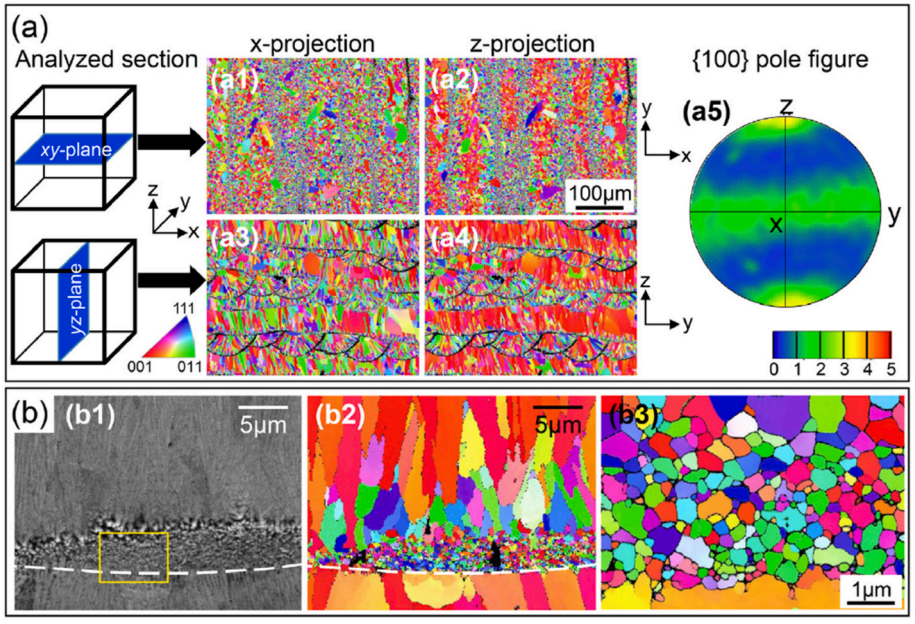

Fig. 9. Microstructure and crystallographic analysis of LPBF-built $Ti_{1.4}Nb_{0.6}Ta_{0.6}Zr_{1.4}Mo_{0.6}$ BioHEA, reprint from Ref. [157]. a) EBSD IPF maps and pole figures along the XY and YZ planes and b) BSE image and corresponding IPF maps where b3 represents a magnified region in b1.

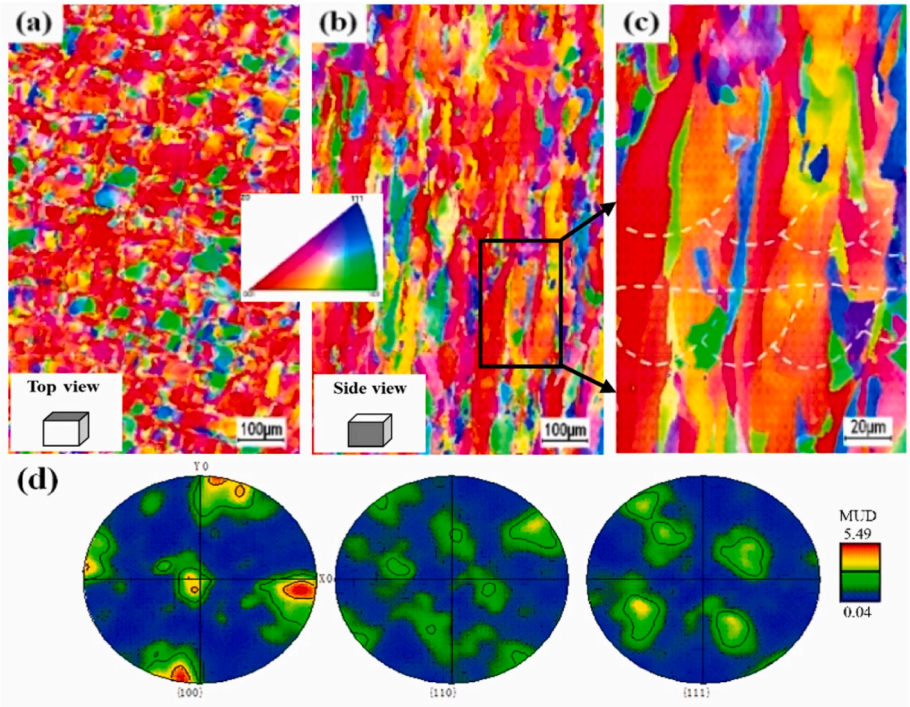

Fig. 10. Texture development of the LPBF-built AlCoCuFeNi HEA in various directions. (a) IPF map along the XY plane, and (b, c) IPF maps along the XZ plane, and (d) PF maps. Reprint from Ref. [68] with permission from Elsevier.

strengthening mechanisms such as twinning. Zhou et al. showed that doped carbon was homogeneously dissolved in the LPBF-built CoCrFeNi HEA [175]. As an interstitial element, carbon improved both yield strength and ultimate tensile strength without degrading any other mechanical properties. Wu et al. and Zhou et al. revealed that C doping led to the formation of nanosized carbides at FCC grain boundaries and C segregation at sub-grain boundaries [173,176]. Park et al. reported the effect of processing parameters and C addition (1 at%) in the LPBF-built

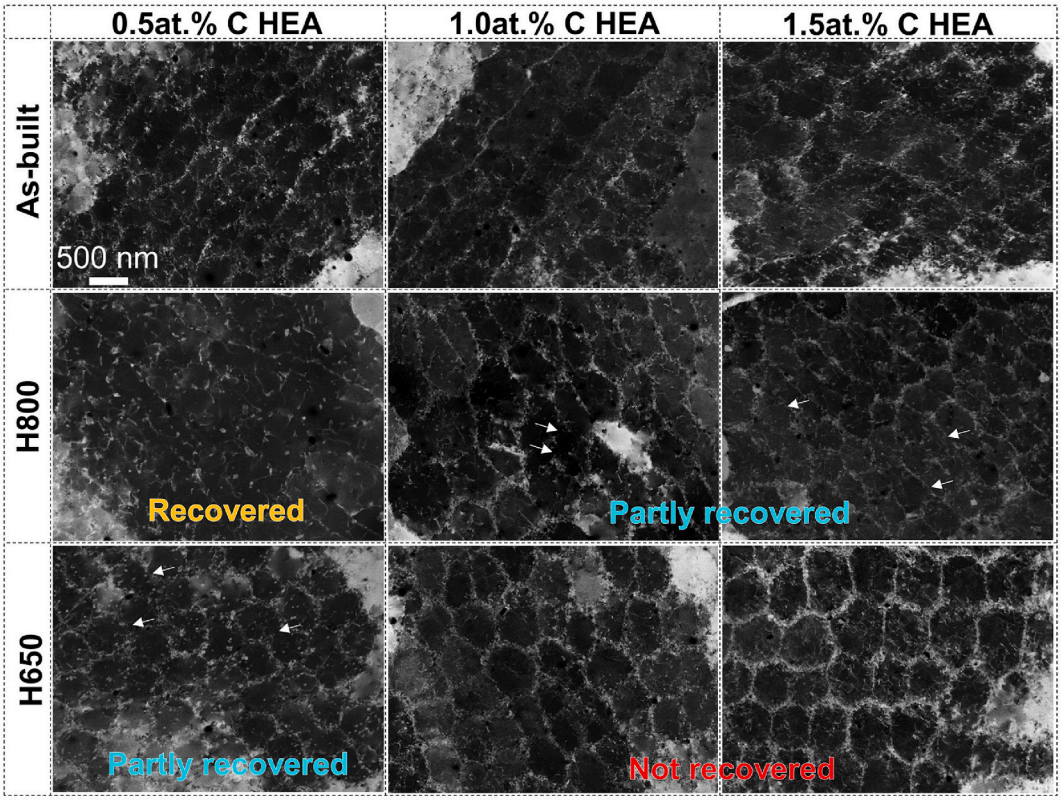

Fig. 11. The microstructure of CoCrFeMnNiCx HEAs produced by LPBF and after aging treatments. Reprint from Ref. [72] with permission from Elsevier.

CoCrFeMnNi, in which C caused both interstitial solid solution strengthening and precipitate formation [177]. Kim et al. recently showed that post-process treatments are beneficial to re-engineering the microstructure of the C-doped CoCrFeMnNi alloy [72]. Partial or full recovery of dislocations after aging at 650 °C and 800 °C stabilized the sub-grain structure, which changed the deformation mechanism and strengthening behavior of LPBF-built CoCrFeMnNiC_x HEAs (Fig. 11).

Song et al. showed that N-doped HEAs formed heterogeneous structures, leading to excellent mechanical properties due to grain refinement, lattice distortion and dislocation impingement in the LPBF-built CoCrFeNi HEA [178]. Wang et al. also investigated the effect of doping nitrogen into the CoCrFeNi HEA [178]. It was revealed that grain orientation played an important role in enhancing mechanical performance. Nanotwins were activated in the grains oriented close to <111> and <110>, whereas slip bands were mostly observed in the grains oriented close to <100> (Fig. 12).

4.2. Multi-phase HEAs

Most of the HEAs that have been produced and studied are multi-phase alloys, although HEAs were initially proposed as single-phase. The generally better mechanical properties of multi-phase HEAs compared to single-phase HEAs motivate an increasing number of studies focusing on multi-phase HEAs. Specifically, it would be interesting to study AM-ed multi-phase HEAs, since the microstructure of AM-ed HEAs, including the size and distribution of secondary phases, can be manipulated more easily by changing the processing parameters, compared to that for HEAs produced by conventional routes.

Al_xCoCrFeNi alloys belong to the most studied single- or multi-phase HEAs. FCC precipitates were seen to form in the BCC_B2 matrix of the EPBF-built AlCoCrFeNi HEA [16,132,133]. EPBF-built alloys contained a relatively higher content of FCC phase compared to the as-cast counterparts. Rapid cooling achieved by EPBF promoted the precipitation of FCC phase mostly at the boundaries of BCC_B2 grains; thus, the growth of prior BCC_B2 grains was restricted. The content of FCC phase was almost four times higher at the bottom than at the top section of the as-built parts: the bottom part was exposed to subsequent melting/-cooling and continuous pre-heating, favoring the solid-state phase transformation from BCC to FCC and the growth of FCC precipitates [132]. The growth of FCC phases also reduced the strong <100> texture of the BCC phase [53,161,180].

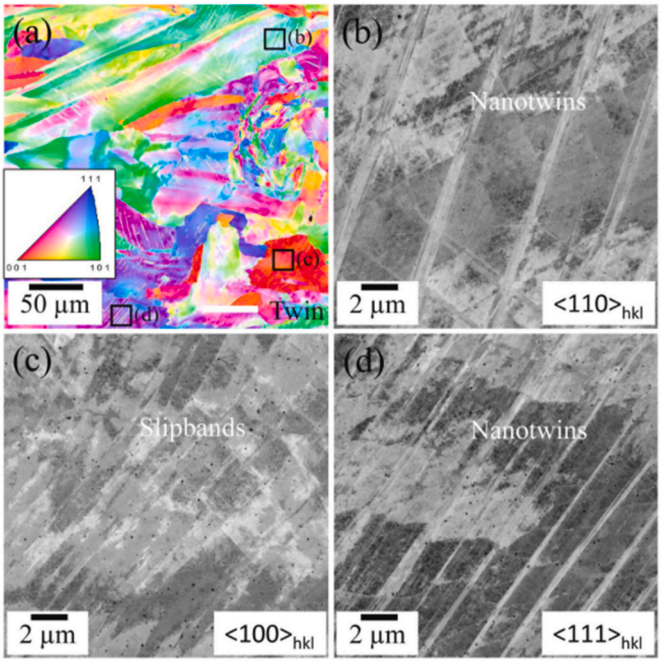

Fig. 12. (a) IPF map of the N-doped FeCoNiCr HEA at a tensile strain of 34 %. White lines indicate the mechanical twins. (b, c, d) ECC images showing the microstructures for the marked grains in (a), which correspond to orientations close to <110>, <100>, and <111>, respectively. Reprint from Ref. [179] with permission from Elsevier.

Wei et al. observed microstructural changes when producing Al_x-CoCrFeNi HEAs by LPBF [135]. The alloy with low aluminum contents (x = 0.07–0.50) consisted of grains formed along the <110> direction, and a single-phase FCC structure was observed. Increasing Al content (x = 0.67–0.78) led to the formation of the BCC phase, with a prominent <100> texture of BCC grains along the building direction. At x = 0.88, the formation of B2 from the BCC matrix eliminated the texture of the BCC phase. Another dual-phase HEA, AlCoCrCuFeNi, was investigated to show the effect of LPBF processing parameters on the microstructural changes. An increased VED promoted the formation of the FCC phase rather than the BCC phase [181]. Contrary to EPBF-built AlCoCrFeNi, the FCC phase was distributed more homogeneously and the grain size was finer in the LPBF-built alloy [181]. Sarswat et al. reported that adding Zr in the AlCoFeNiSmTiVZr system promoted the formation of the BCC phase from the FCC matrix while generating a high lattice strain [182]. Cai et al. observed the formation of (Co, Ni)Ti_2 in the BCC matrix of the AlCoCrNiTiV HEA [183]. Cagirici et al. used EPBF to design and produce CoCrFeNiMn-xTi HEAs containing TCP phases [71]. Having a hot powder cake (~730–780 °C) during printing and Ti doping into the CoCrFeMnNi alloy triggered the nucleation and growth of secondary phases including σ, Laves, and Ni_3Ti, from the FCC matrix (Fig. 13) [71].

4.3. HEA matrix composites

The difficulties of forming homogeneously dispersed secondary phases in AM-ed HEAs motivated a new design strategy: to produce HEA matrix composites. Laser-based PBF and DED techniques have been used to produce ceramic reinforced CoCrFeMnNi HEAs to achieve high material performance for structural applications [73,141,158,184–187]. Li et al. showed that TiN nanoparticles improved the packing density of the pre-alloyed CoCrFeMnNi feedstock and restricted the growth of FCC grains in LPBF-built alloys [141,184,185]. Process optimization efforts revealed that low energy density was not suitable for producing TiN/-CoCrFeMnNi alloys, since it caused microstructural defects such as micro-porosity, key-hole formation and cracks, and improper bonding between TiN and CoCrFeMnNi particles [141]. Tailoring processing parameters resulted in microstructural homogeneity and good metallurgical bonding between TiN particles and CoCrFeMnNi at atomic scale (Fig. 14). Consequently, ultra-fine TiN strengthened alloys yielded outstanding material performance under both tension and compression [184].

CoCrFeMnNi has also been widely used to develop HEA matrix composites, strengthened by TiB_2, TiC, and CeO_2 particles [158,186,187]. Similar to the effect of TiN, both TiB_2 and TiC enhanced the mechanical properties of AM-ed HEAs. High energy induced by LENS helped to improve the densification of the CoCrFeMnNi/TiB_2 HEA matrix composite. Chen et al. developed TiC strengthened CoCrFeMnNi with a hierarchical microstructure, and increased the number of nucleation sites for nanoprecipitates inside the cellular FCC solid solution [158]. Savinov et al. employed LMD to produce the CeO_2 reinforced CoCrFeMnNi [187]. Decomposition of CeO_2 particles upon laser exposure formed irregularly shaped oxides, which were enriched with Cr and Mn. The study showed that newly formed oxides, before the solidification of the FCC matrix, varied the orientation of FCC grains. However, the strong <001> texture could not be eliminated [187].

In addition to inducing ceramic particles to the pre-alloyed CoCrFeMnNi HEA, Guan et al. proposed forming a laminated HEA, alternating CoCrFeMnNi and AlCoCrFeNiTi layers and aiming for strength-plasticity synergy [188]. The FCC/BCC laminated structure boosted the material performance, partially because a good metallurgical

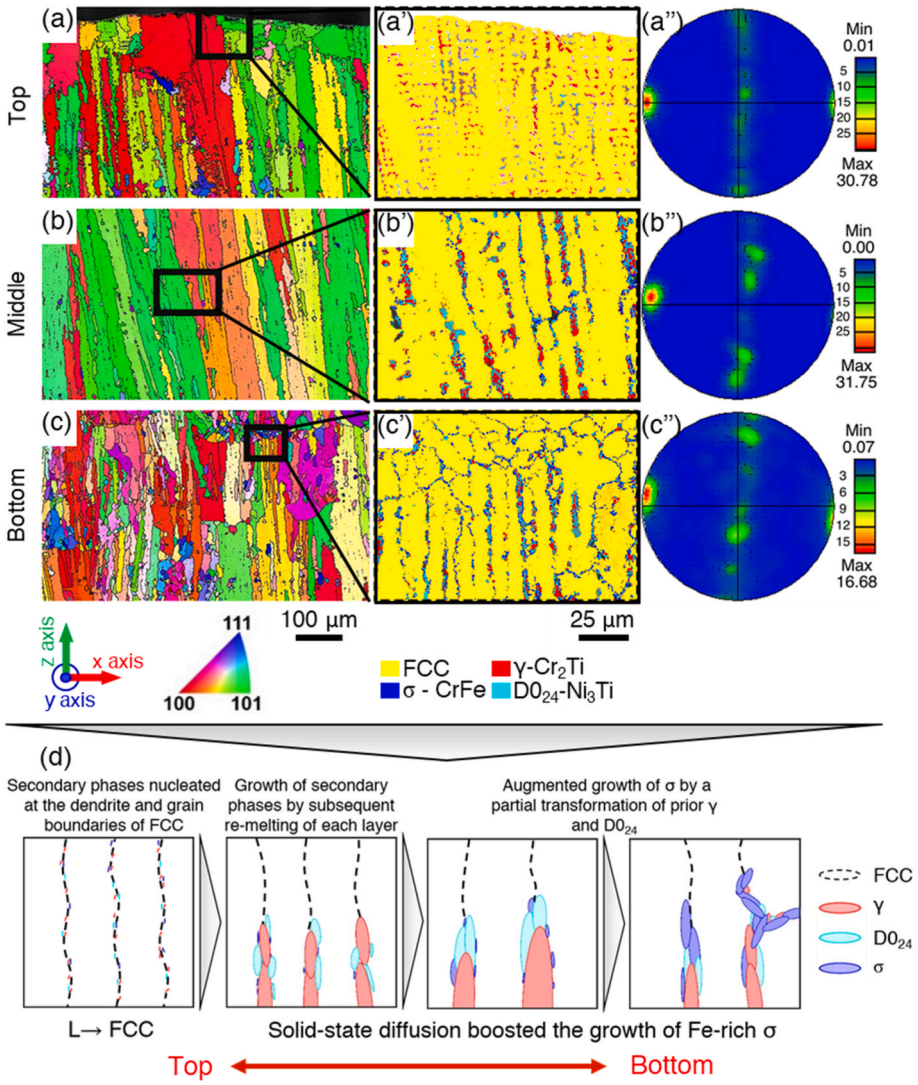

Fig. 13. Microstructural variation along the building direction in the EPBF-built CoCrFeMnNi-0.18Ti. (a, b, c) EBSD IPF maps, (a', b', c') phase maps, (a″, b″, c″) pole figures with the texture index, and (d) graphical illustration of the phase evolution. Adapted from Ref. [71] with permission from Elsevier.

bonding between different layers was achieved (Fig. 15) [188]. A similar approach was also used when developing a FeCoCrNi/FeCoCrNiAl laminated HEA by LMD [51]. Recently, Fe-based metallic glasses were introduced into the AlCoCrFeNi HEA using LPBF [73]. Adding 5 % Fe-based metallic glasses eliminated the preferential growth of BCC grains in AlCoCrFeNi while promoting FCC phase formation [73].

5. Mechanical properties of AM-ed HEAs

5.1. Hardness

Microhardness measurements can be used to quickly benchmark the performance of AM-ed HEAs, and the microhardness results of AM-ed HEAs are summarized in Table 1. It is observed that, in general, HEAs such as CoCrFeMnNi and AlCoCrFeNi produced by EPBFhave relatively lower hardness compared to that produced by BJP, LPBF, and DED, because of the slower cooling rate obtained by EPBF. The fine-grained microstructure achieved by the latter techniques led to higher hardness. The microhardness of AM-ed CoCrFeMnNi HEAs, which contain only the FCC solid solution, ranges from 157 to 300 HV. A higher hardness could be obtained by introducing sub-surface defects (over 300 HV) [9] and *in situ* alloying (261 ± 7 HV) [116] in the LPBF-built CoCrFeMnNi. Chen et al. [116] assumed that the higher oxygen content in the feedstock produced via *in situ* alloying promoted the formation of oxygen complexes, which further increased the hardness of the alloy. The microhardness of AM-ed AlCoCrFeNi ranges from 270 to 633 HV. Niu et al. reported that the highest hardness for that particular alloy was achieved using a high VED of 111.1 J/mm^3, which resulted in a fine grain size [189]. Meanwhile, a high density of dislocations formed in the BCC phase of AlCoCrFeNi improved the resistance of the alloy to external loads. In addition, Karlsson et al. [99] investigated the effect of post-process heat treatments on the BJP-ed AlCoCrFeNi alloy and revealed that the σ phase is the main contributor to high hardness in the as-sintered alloy. On the other hand, post-process heat treatments reduced hardness when transforming the σ phase to FCC at the heat treatment temperature of 1000 °C but increased hardness when eliminating the FCC phase at the heat treatment temperature of 1200 °C.

Some refractory HEAs, such as NbMoTaW and TiZrNbHfTa, and HEAs/carbide composites, such as AlCoCrCuFeNi/WC, have higher hardness than other HEAs regardless of the AM techniques [88,174,196]. The reasons for the higher hardness in single-phase refractory HEAs are ascribed to their refined and uniform microstructure, as well as the intrinsic superior properties of refractory metals over other 3D transition metals [203]. Li et al. improved hardness in LPBF-built AlCoCrCuFeNi by adding WC [196]. The content of carbide precipitates changed according to the chemical composition of the HEA

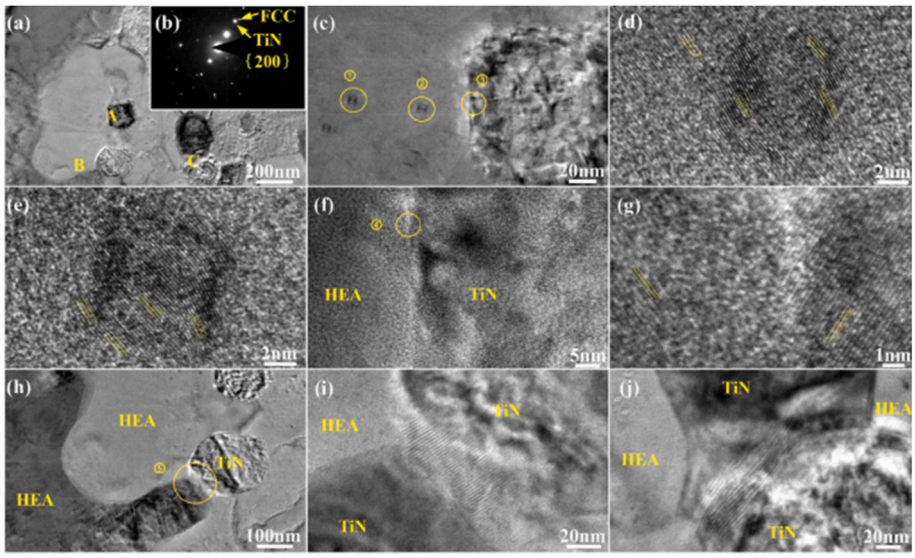

Fig. 14. TEM images of the LPBF-built TiN_p/HEA composite. (a) A typical micro-region with its SAED pattern; (b) enlargement of region "A" with (c) further enlargement at the circled regions (d) ①, (e) ②, (f) ③and (g) ④; (h) enlargement of region "B" with (i) further enlargement at the circled regions ⑤ and (j) enlargement at region "C". Note: the marked parallel lines illustrate the atomic rows. Reprint from Ref. [185] with permission from Elsevier.

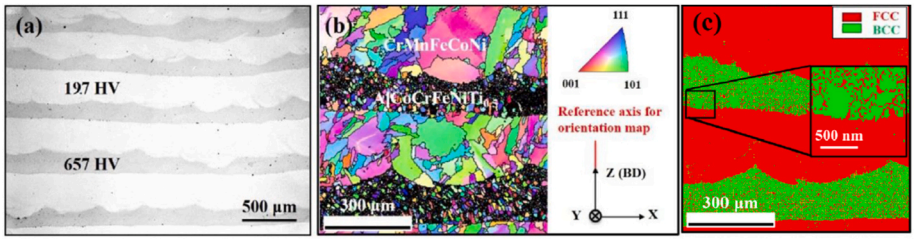

Fig. 15. Microstructure of a laminated HEA matrix composite, CrMnFeCoNi/$AlCoCrFeNiTi_{0.5}$, produced by LENS. (a) OM image of the laminated composite showing representative microhardness, (b) EBSD IPF map of alternating coarse and fine grains, and (c) EBSD phase map along the building direction [188]. Reprint from Ref. [188] with permission from Elsevier.

phase. Decreasing the contents of major constituents, Fe and Ni, increased the hardness of the AlCoCrCuFeNi/WC composite. On the other hand, variation in the type of carbides, i.e., WC or W_2C, also modified the hardness of the composite.

5.2. Tensile properties

5.2.1. Room temperature

Fig. 16 shows that the tensile properties of AM-ed CoCrFeMnNi are slightly better than that of as-cast counterparts in terms of having finer microstructure, pronounced texture, and increased resistance to dislocation motions, resulting in enhanced yield strength. Early research using DED techniques such as LMD and LENS, as well as the LPBF method, has shown that higher yield strength can be achieved compared to other AM techniques. This is due to the rapid solidification of molten metals, which introduces a high density of dislocations in the as-built structures. Although the rapid solidification and the resultant fine grain structures increased yield strength, the relatively slower cooling rates obtained in EPBF provide better ductility compared to the ones produced by other AM techniques by eliminating the strong texture. Zhu et al. reported that the hierarchical dislocation distribution at the cell walls in the microstructure of CoCrFeMnNi produced by LPBF enhanced its mechanical properties under tension; however, exceptional grain boundary hardening shaded the effectiveness of strengthening gained by the cell walls and sub-grain boundaries [110]. Wang et al. produced CoCrFeMnNi with the highest ductility by promoting nano-twinning and restricting the movement of dislocations in as-built structure [70]. The contribution of twinning was limited in this case, however, since the formation of twins was strictly regulated by the crystal orientation of columnar grains achieved via EPBF [70]. In addition to the main differences, such as grain morphologies and boundaries, observed on CoCrFeMnNi HEAs manufactured via LPBF, EPBF and DED methods, resultant texture also affected the mechanical properties based on anisotropy. Although existing studies proved that microstructural anisotropy created via PBF techniques manifest a positive change in room temperature tensile properties as compared to the ones fabricated via DED, the tensile test conditions, which are built-test orientation, sample size-shape effect, and strain rate effect, must be evaluated critically considering an application. Anisotropy and larger-grained structures in DED-built CoCrFeMnNi HEAs usually resulted in having lower yield strength due to the limited strengthening [55,116,204].

The mechanical properties of interstitial HEAs are shown in Fig. 16-(b, b'). The precipitation of carbon atoms along the grain boundaries of the LPBF-built CoCrFeMnNi improved tensile performance. Introducing carbon atoms into the material also strengthened grain boundary while limiting grain growth [177]. Wang et al. addressed the role of nitrogen dopant in the CoCrFeNi alloy: Adding nitrogen achieved a hierarchical structure that contained a dislocation network and low angle grain boundaries [179]. The hierarchical structure also led to the creation of twins and limited dislocation motion, thereby increasing both the strength and ductility of LPBF-built CoCrNiFe-1.8 at% N alloy.

Multi-phase HEAs show relatively different characteristics to single-phase or interstitial HEAs. The coherency or semi-coherency created between FCC-BCC, FCC-HCP or BCC-HCP phases, as well as a mixture of

Table 1
Microhardness of AM-ed HEAs.

Material	Phase Constituents	AM Technique	Hardness (HV)	Ref.
CoCrFeNi	FCC	LPBF	205–238	[44]
CoCrFeNi	FCC	LPBF	259 ± 8	[190]
CoCrFeNi	FCC	LPBF/HT[a] (800 °C)	209 ± 12	[190]
CoCrFeNi	FCC	LPBF	~260	[54]
CoCrFeNi	FCC	LPBF	187–196	[191]
$CoCrFeNiC_{0.05}$	FCC	LPBF	340	[176]
CoCrFeMnNi	FCC	LPBF	261 ± 7	[116]
CoCrFeMnNi	FCC	LPBF	200–300	[9]
CoCrFeMnNi	FCC	LPBF	212	[192]
CoCrFeMnNi	FCC	EPBF	157.1 ± 4.5	[70]
CoCrFeMnNi	FCC	DED	195	[165]
CoCrFeMnNi	FCC	DED	~194.2	[169]
$CoCrFeMnNiTi_x$	FCC/BCC/σ	DED	182–973	[193]
$CoCrFeMnNiTi_x$	FCC/σ/γ/η	EPBF	460–900	[71]
AlCoCrFeNi	FCC/BCC-B2/σ	BJP	530	[99]
AlCoCrFeNi	FCC/BCC-B2	BJP/HT[a] (1000 °C)	418	[99]
AlCoCrFeNi	BCC-B2	BJP/HT[a] (1200 °C)	500	[99]
AlCoCrFeNi	FCC	LPBF	270	[48]
AlCoCrFeNi	BCC-A2/BCC-B2	LPBF	632.8	[189]
AlCoCrFeNi	FCC/BCC-B2	EPBF	389–495	[132]
AlCoCrFeNi	BCC-B2	DED	543	[89]
AlCoCrFeNi	BCC-A2/BCC-B2/$L1_2$	DED	520–628	[194]
AlCoCrFeNi	BCC-B2	DED	538	[49]
$Al_{0.3}$CoCrFeNi	FCC	DED	155.7 ± 10.2	[195]
$Al_{0.7}$CoCrFeNi	FCC/BCC-B2	DED	415.2 ± 13.3	[195]
$Al_{0.3}$CoCrFeNi	FCC	DED	208.8 ± 3.5	[159]
$Al_{0.3}CoCrFeNi_{1.7}$	γ	DED	149–163	[194]
$Al_{0.7}CoCrFeNi_{1.3}$	γ/B2	DED	271–308	[194]
$Al_{1.7}CoCrFeNi_{0.3}$	BCC-A2/BCC-B2	DED	649.671	[194]
$AlCoCrFeNi_{2.1}$	FCC/BCC	LPBF	~380	[74]
AlCoCuFeNi	BCC-B2	LPBF	541	[68]
AlCoCuFeNi	FCC/BCC-B2	LPBF/HT[a] (900 °C)	406	[68]
AlCoCuFeNi	FCC/BCC-B2	LPBF/HT[a] (1000 °C)	399	[68]
$AlCoFeNiV_{0.9}Sm_{0.1}$	FCC	LPBF	~1076	[182]
AlCoFeNiTiVZr	FCC	LPBF	~124	[182]
$AlCoFeNiSm_{0.05}TiV_{0.95}Zr$	Al-Sm/Al_3V/Al_3Zr/$(Fe,Al)_2Zr$	LPBF	~720	[182]
$AlCoFeNiTiV_{0.9}Sm_{0.1}$	FCC	LPBF	~375	[182]
$AlCrFeMoV_x$ (0 < x < 1)	BCC	DED	485–581	[11]
AlCoCrCuFeNi/WC	FCC/WC/W_2C/η	LPBF	711.7–1413.4	[196]
$AlMo_{0.5}NbTa_{0.5}TiZr$	BCC-B2/HCP	DED	646.4 ± 15.7	[197]
$Ni_{2.1}CoCrFe_{0.5}Nb_{0.2}$	FCC	DED	260	[198]
$Ni_{32}Co_{30}Cr_{10}Fe_{10}Al_{18}$	FCC/BCC-B2	DED	317	[199]
NbMoTaW	BCC	LPBF	826	[174]
NbMoTaTiNi	BCC-B2	LPBF	621	[200]
TiZrNbHfTa	BCC	DED	~509	[88]
$Ti_{21.2}Zr_{1.4}Nb_{54}Ta_{23.4}$	BCC	DED	230	[201]
$Ti_{21.6}Zr_{54.2}Nb_{0.2}Ta_{24}$	BCC	DED	310	[201]
WMoTaNbC	BCC/Nb_2C	EPBF	720	[202]

[a] Annealing treatments.

various forms of ordered and disordered FCC and BCC mixtures in these multi-phase HEAs, increased strength considerably. Their ductility, however, could not be improved simultaneously (Fig. 16c). Improvement to the ductility of multi-phase HEAs could alternatively be achieved via post-process heat treatments, such as HIP, to obtain a superior strength-ductility balance [20,67,92,170]. As a representative example of multi-phase HEAs, eutectic HEAs show excellent strength and ductility in as-built conditions [74,152,161,205]. Wang et al. reported that the LPBF-built $AlCoCrFeNi_{2.1}$ HEA has yield strength, ultimate tensile strength, and elongation to failure of ~1.1 GPa, ~1.4 GPa, and 13.7 %, respectively [161]. Similarly, Ren et al. demonstrated that LPBF-built AlCoCrFeNi2.1 EHEA with a unique hierarchical microstructure, including nanoscale dual-phase (fcc and bcc) lamellar eutectic colonies with exceptionally thin lamellar thicknesses, unlike the thicker microlamellae in conventional EHEAs, exhibits superior mechanical properties compared to those reported by Wang et al. [205]. The better mechanical properties having a yield strength of >1.3 GPa with a significant ductility could also be attributed to randomized orientations of the eutectic colonies [205]. Another eutectic HEA, $Ni_{30}Co_{30}Cr_{10}Fe_{10}Al_{18}W_1Mo_1$, showed yield and ultimate tensile strength of 1.0 GPa, and 1.4 GPa at room temperature, respectively [152]. Ultra-fine lamellar structure, consisting of FCC and B2, contributed to achieving this combination of properties. In addition to the eutectic HEAs, recent research on manufacturing various refractory HEAs (RHEAs) showed that ductility could be gained by phase engineering. Gou et al. reported that TiZrHfNb RHEA with varying niobium (Nb) content achieved exceptional tensile yield strengths exceeding 1000 MPa while retaining significant ductility [153]. Notably, the TiZrHfNb RHEA exhibited a remarkable yield strength of 1048 MPa and ductility of 10 % in the optimal loading direction. Same alloy also achieved a yield strength of 1034 MPa and an impressive 18.5 % ductility when loaded horizontally [153].

5.2.2. Low temperature

LMD-built CoCrFeMnNi showed superior tensile strength at cryogenic temperatures compared to room temperature. Qui et al. reported that yield strength and ultimate tensile strength of the single-phase CoCrFeMnNi improved by 60 % and 65 % respectively, whereas the elongation to failure increased by 38 % at 77K compared to those at room temperature [14]. Although the increase in strength of CoCrFeMnNi HEA reported by Qui et al. was significant, Xiang et al. reported lower strength but higher ductility for the same alloy manufactured via LMD. Higher energy accumulation leading to an increase in the grain size of single-phase FCC structure resulted in having ultimate tensile strengths and elongations of 610 MPa, 73 % and 878 MPa, 95 % at 200K and 77K, respectively [206]. Li et al. reported similar mechanical properties at 77K for LMD-built Cantor alloy. Additionally, they investigated the tensile properties of Fe-rich $(CoCrFeMnNi)_{50}Fe_{50}$ HEA, which has an ultimate tensile strength of 925 MPa and elongation of 60 % at 77K due to strain-induced FCC to BCC phase transformations [207]. In contrast to CoCrMnFeNi HEAs produced via LMD, LPBF yielded superior mechanical properties both at room and cryogenic temperatures by minimizing the grain size and introducing more dislocation and providing tailorable microstructure throughout manufacturing process. Kim et al. showed that Cantor alloy strengthened via nano-oxides through LPBF has yield strength, tensile strength and elongation of 1150 MPa, 1450 MPa and 23.4 % at 77K, respectively [208]. The superior tensile properties of LPBF-built $Co_{23}Cr_{21}Fe_{21}Ni_{35}$ MEA having a yield strength of 0.75 GPa and elongation of ~53 % at 123K were also reported by Kuzminova et al. [209]. In addition to single-phase MEA and HEAs, Yang et al. achieved outstanding mechanical properties in the eutectic $Ni_{30}Co_{30}Cr_{10}Fe_{10}Al_{18}W_1Mo_1$ HEA via LPBF [152]. The alloy even maintained exceptional tensile properties at low and medium temperatures. The yield strength and ultimate tensile strength of the eutectic HEA are ~1.2 GPa and ~1.5 GPa at −196 °C, respectively [152].

5.2.3. Medium and high temperature

Additively manufactured MEAs/HEAs as compared to conventionally manufactured counterparts showed better tensile properties not only at room temperature but also at elevated temperatures. Smith et al. reported that LPBF-built nano-oxide dispersion strengthened (ODS)-

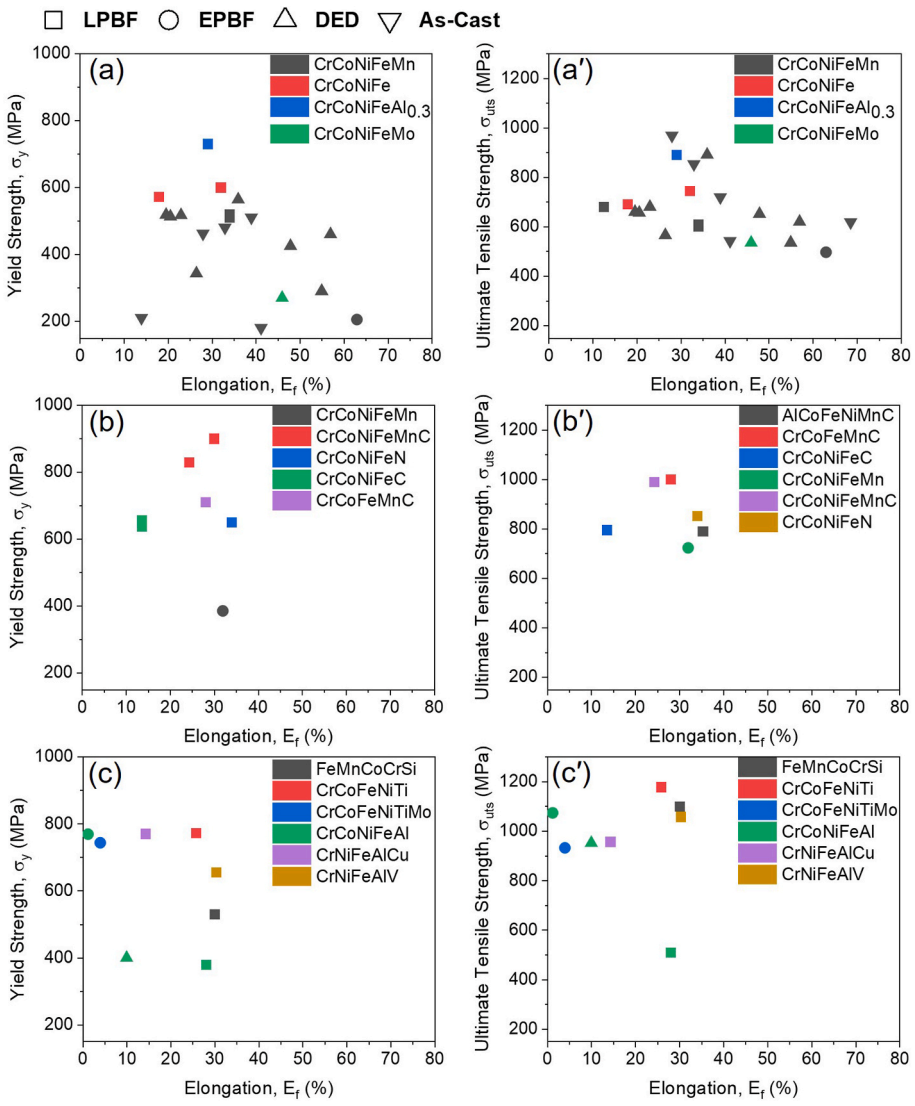

Fig. 16. Room temperature tensile properties of (a, a') single-phase, (b, b') interstitial HEAs, and (c, c') multi-phase HEAs. Data reanalysed from Refs. [8,10,20,21,42,57,60,74,99,120,125,135,139–141,144,148,149,167].

CoCrNi (ODS-GRX810) has a higher tensile strength (~128 MPa) at 1093 °C compared to pure CoCrNi (non ODS-GRX810), which has a tensile strength of ~120 MPa [210]. Incorporating Y_2O_3 particles into CoCrNi resulted in a substantial increase in strength and a remarkable doubling of ductility compared to the non-ODS CoCrNi MEA. Yang et al. studied the eutectic alloy, $Ni_{30}Co_{30}Cr_{10}Fe_{10}Al_{18}W_1Mo_1$, manufactured via LPBF, which displayed good strength-ductility balance (yield strength of ~0.6 GPa and fracture strain of ~15 %) at 650 °C; however, the alloy significantly lost its strength (yield strength of ~0.26 GPa and fracture strain of ~29 %) at 760 °C due to the ductile to brittle transition of B2 phase [152]. Li et al. revealed that LMD-built single-phase CoCrFeMnNi and its composite doped with 5 wt% WC both have reasonable strength and ductility at 600 °C. Although the decrease in yield strength for pure HEA was remarkable, WC-induced HEA matrix composite owned a yield strength of 220 MPa, ultimate tensile strength of 405 MPa and elongation of 45 % at 600 °C [211]. Jeong et al. reported that tensile properties of TiNbCrVNi HEA manufactured via L-DED show improvement in terms of ductility at elevated temperatures (800 °C–1000 °C) up to the elongation of ~55 % at 1000 °C; however, the yield and ultimate tensile strength of AM-ed alloy decrease drastically to 80 MPa and 260 MPa, respectively. The decrease in yield strength reached to ~90 % of that at room temperature due to the melting of BCC B2 phase at 980 °C [212].

It should also be noted that the investigation of tensile properties of refractory HEAs produced with AM techniques is challenging mainly due to the brittleness of the produced alloys at room temperature. Thus, only a few reports has been published to the date that investigates tensile properties of AM-ed RHEAs, according to the literature [153]. Although these alloys produced by conventional or AM techniques showed superior compressive properties at high temperatures, having limited ductility at room temperature in the as-cast form brings challenges when investigating their tensile properties [46,50].

5.3. *Compressive properties*

Although tensile properties are more meaningful for engineering, studies on the compressive properties of AM-ed HEAs are also necessary, since many of them have relatively low or even no tensile ductility compared to their counterparts produced by conventional routes. Furthermore, it is important to understand the anisotropy in the mechanical properties of AM-ed HEAs in order to apply them in engineering applications, where the materials might work under both tensile and compressive loading. Indeed, great effort has been made to characterize the compressive properties of various HEAs, especially the $Al_xCoCrFeNi$

system. The lower Al variants, such as $Al_{0.3}$CoCrFeNi, form a single-phase FCC structure. The compressive yield and fracture strength of $Al_{0.3}$CoCrFeNi are relatively weak compared to $Al_{0.6}$CoCrFeNi, $Al_{0.85}$CoCrFeNi, and AlCoCrFeNi, since the BCC structure formed in the latter alloys typically has a higher strength than that of the FCC structure [16,47,99,195]. The effect of HIP and heat treatments on the compressive properties have also been explored for Al_xCoCrFeNi HEAs [99,170]. HIP slightly decreased compressive yield strength while increasing the compressive malleability of AM-ed alloys. Annealing treatment, however, increased the yield strength of AlCoCrFeNi printed by BJP. The compressive properties of LPBF-built CoCrFeMnNi and AlCrCuFeNi HEAs were also investigated [122,123,213,214]. In two different works, Niu et al. and Kim et al. revealed that as-printed CoCrFeMnNi have compressive yield strength of 492 MPa and 704 MPa as well as maximum compressive strains of 70 % and 40 %, respectively [213,214]. The compressive yield strength of AM-ed HEAs is listed in Table 2. The maximum compressive strength and compressive strain, however, are not listed due to the non-standardized tests that were used in the literature.

6. Corrosion resistance

Corrosion-resistant metallic alloys have been developed and investigated extensively since corrosion resistance is a critical attribute for materials in some engineering applications, when the materials are exposed to the harsh environment directly. The corrosion resistance of materials has been benchmarked in terms of various electrochemical parameters, including corrosion potential (E_{corr}), pitting potential (E_{pit}), and corrosion current density (I_{corr}). Recent studies have revealed that the corrosion resistance of HEAs produced by conventional manufacturing routes are comparable with that of austenitic stainless steels, and are nobler than aluminum alloys and carbon steels [216–218]. Studies have also indicated that the presence of Cr, Mo, and Ti in HEAs increases the corrosion resistance, whereas that of Al, Cu, and B decreases it [217]. Compositional variations, such as elemental segregation or the formation of intermetallics, can cause localized corrosion and hence degradation of the corrosion resistance [219,220]. Only a few studies have characterized the corrosion resistance of AM-ed HEAs. A summary of the electrochemical parameters of those investigated alloys is given in Table 3. Kuwabara et al. demonstrated that the SEM-ed AlCoCrFeNi has inferior corrosion resistance than that of the as-cast AlCoCrFeNi and SS304, because of the phase separation [133]. Cr-deficient regions, where Al and Ni were enriched, were susceptible to pitting corrosion. Dada et al. observed that Ti or Cu doped AlCoCrFeNi HEAs, which were produced via LMD, have better corrosion resistance compared to undoped ones and some of the Al-free CoCrFeNi-based HEAs [221,222]. Although Ti or Cu doped AlCoCrFeNi HEAs showed better corrosion resistance, it was suggested that secondary phases or intermetallics might cause localized corrosion. Therefore, corrosion-susceptible intermetallics should be suppressed when designing the alloy compositions and selecting the processing parameters of the employed AM techniques. Sarswat et al. revealed that Zr-containing HEAs, i.e., AlCoFeNiTiVZr and $AlCoFeNiSm_{0.05}TiV_{0.95}Zr$, have better corrosion resistance than Zr-free HEAs [182]. However, in both Zr-free and Zr-doped LPBF-built HEAs, the phase separation promoted the galvanic couple formation, and the corrosion resistance of designed HEAs is therefore worse than that of stainless steels [182]. Zhang et al. reported that Nb-, Mo-, and Ta-containing HEAs, designed for marine applications, have better corrosion resistance than SS 316L, although a low level of compositional segregation in the LPBF-built NbMoTaW caused pitting corrosion with a depth of 1 mm [174].

Table 2
Compressive yield strength of AM-ed HEAs.

Material	AM Technique	Compression Sample Geometry	Compressive Yield Strength (MPa)	Ref.
AlCoCrFeNi	EPBF	Cylindrical	1015 ± 52.5	[16]
$Al_{0.3}$CoCrFeNi	DED	Cylindrical	194	[47]
$Al_{0.3}$CoCrFeNi	DED/HIP	Cylindrical	183	[170]
$Al_{0.6}$CoCrFeNi	DED	Cylindrical	~400	[47]
$Al_{0.6}$CoCrFeNi	DED/HIP	Cylindrical	~400	[170]
$Al_{0.85}$CoCrFeNi	DED	Cylindrical	~1400	[47]
$Al_{0.85}$CoCrFeNi	DED/HIP	Cylindrical	1300	[170]
AlCoCrFeNi	BJP/HT[a] (1000 °C)	Cylindrical	1203 ± 22	[99]
AlCoCrFeNi	BJP/HT[a] (1200 °C)	Cylindrical	1461 ± 23	[99]
$Al_{0.3}$CoCrFeNi	DED	Cube/DC[b]	~200	[195]
$Al_{0.7}$CoCrFeNi	DED	Cube/DC[b]	878	[195]
CoCrFeMnNi	LPBF	Cylindrical	490–498	[213]
CoCrFeMnNi	LPBF	Cylindrical	704–770	[214]
MoNbTa	DED	Cylindrical	874	[215]
$MoNbTaW_{0.16}$	DED	Cylindrical	840	[215]
$MoNbTaW_{0.33}$	DED	Cylindrical	895	[215]
$MoNbTaW_{0.53}$	DED	Cylindrical	890	[215]
MoNbTa	DED	Cylindrical[c]	530 (@1000 °C)	[215]

[a] Annealing treatments.
[b] Dynamic compression.
[c] High-temperature test.

Table 3
Electrochemical parameters of AM-ed HEAs.

Material	Solution	E_{corr} (V)	Log I_{corr} (A/cm2)	Ref.
AlCoCrFeNi	3.5 wt% NaCl	−0.355	−5.84	[133]
AlCoCrFeNiCu	3.5 wt% NaCl	−0.702	−7.14	[222]
AlCoCrFeNiTi	3.5 wt% NaCl	−0.465	−7.12	[222]
AlCoFeNiTiVZr	3.5 wt% NaCl	−0.755	−4.44	[182]
$AlCoFeNiSm_{0.05}TiV_{0.95}Zr$	3.5 wt% NaCl	−0.666	−4.96	[182]
$AlCoFeNiTiV_{0.9}Sm_{0.1}$	3.5 wt% NaCl	−0.655	−5.08	[182]
$AlCoFeNiV_{0.9}Sm_{0.1}$	3.5 wt% NaCl	−0.628	−5.17	[182]
NbMoTaW	3.5 wt% NaCl	−0.242	−8.05	[174]
CoCrFeNi	0.5 M H_2SO_4	–	0.785	[223]
CoCrFeMnNi	3.5 wt% NaCl	−0.189	−7.05	[221]
$CoCrFeNiMo_{0.2}$	3.5 wt% NaCl	−0.192	−8.73	[224]
CrFeCuTiV	3.5 wt% NaCl	−0.084	−4.94	[22]

7. Applications of AM-ed HEAs

Recent advances in the development of HEAs revealed that these innovative alloys could replace existing materials while offering superior performances in various fields, such as energy storage, biomedical, aerospace, marine, and nuclear applications.

The development of multi-functional materials for energy storage applications became critical considering the global energy trends toward clean energy [225,226]. Hydrogen is one of the most popular renewable energy sources, thus its storage is critical in terms of engineering design. Hydride forming metallic elements, compounds and alloys makes hydrogen storage safer [225]. BCC-based HEAs supported by various intermetallics, such as in the types of AB_2 and AB_3, are capable of forming hydrides that absorb significant amounts of hydrogen relative to their weight. For instance, Ti_2CrNbV, TiVZrNb, TiVZrNbHf and Ti_3ZrV_2Nb HEAs have been extensively studied for their hydrogen storage properties [225,227]. Most of the studies focused on the alloys manufactured via conventional processes; however, some studies reported that Ti_2CrNbV and CoCrFeMnNi HEAs manufactured

via LPBF and EPBF, have hydrogen storage capacities of 4.4 and 2.4 wt% at room temperature, respectively [57,227]. Although these alloys showed a potential for hydrogen storage applications, they could not be optimum materials for this application since their hydrogen storage capacity is relatively low in terms of material density.

HEAs are also promising materials for biomedical applications due to their excellent biocompatibility, thermal stability and corrosion resistance. Some of the recent studies named HEAs used for biomedical applications as Bio-HEAs [157,228]. Non or low cytotoxicity of RHEAs, containing Ti, Ta, Nb, V, Mo, Hf, Zr, and W, make these alloys an outstanding candidate for producing implants and surgical tools [157, 228]. The development of new alloys, containing Cu, Zn and Ag, yields additional antibacterial properties to these HEAs, such as CoFeCrCu and CrFeNiCuSi [228–230]. The functional properties of Bio-HEAs form the basis of alloy selection for biomedical applications; however, the mechanical properties have critical importance to compare and replace these novel materials with existing biomaterials. Mostly, Bio-HEAs, which consist of single phase BCC structure, have Young's modulus of 105–260 GPa and yield strength of 820–1700 MPa [228]. Although most of Bio-HEAs have been developed and produced following conventional manufacturing techniques, recent studies reported that AM is also an auspicious technique while producing Bio-HEAs [157,231–233]. TiTaNbMoZr and TiZrHfNbTaMo were successfully fabricated while tailoring their microstructure and mechanical properties via DED and LPBF techniques [231–233].

HEAs suitable for applications in aerospace and marine require high strength and toughness, thermal stability, processability, and excellent corrosion resistance due to the extreme environment they are exposed to during service. Despite the fact that having all these properties at the same time is challenging, the advances in alloy development showed that HEAs with tailored microstructure and specific properties might overcome this challenge. CoCrNi and its derivatives, which consist of either single-phase FCC or nano precipitate/oxide strengthened FCC structures, show outstanding strength and toughness at cryogenic temperatures, which makes them the most suitable candidates for space applications [13,14,18,34,208,210,234–238]. Gludovatz et al., Kumar et al. and Liu et al. revealed exceptional fracture toughness properties of CoCrNi and CoCrNiFeMn alloys at 77K and 20K [13,235,238,239]. The most recent study showed a progressive synergy of nano twinning, dislocation glide, stacking fault formation and phase transformations cause having a crack-initiation fracture toughness of 459 MPa $m^{1/2}$ and a crack-growth toughness of 540 MPa $m^{1/2}$ on CoCrNi MEA at 20K [235]. The studies focused on the fabrication of the same alloys via DED-LB and LPBF also revealed comparable mechanical performance at 210K, 196K and 77K [206,240,241]. In addition to the cryogenic temperatures, ODS HEAs, such as CoCrNi + Y_2O_3 produced via LPBF and CoCrNiFeMn + Y_2O_3 produced via mechanical alloying, exhibit formidable mechanical performance at high temperatures while keeping high thermal stability [210,242]. Smith et al. proved that Y_2O_3-strengthened CoCrNi alloy manufactured via LPBF has superior mechanical properties, which are tensile strength of ~120 MPa and fracture strain of ~35 % than other Ni-superalloys (IN 718 and IN 625) at 1093 °C [210]. Moreover, CoCrNiMoW, TiAlNbV and TiNbTaZrHf HEAs have promising mechanical performance to replace existing counterparts for aerospace and marine applications. These alloys produced by employing additive manufacturing might further be subjected to development and implemented in the mainstream fabrication of engine components, turbine blades, submarine hulls, and ship propellers.

The tuneable mechanical properties, high thermal stability, and corrosion resistance make HEAs promising candidates while fulfilling the emerging demands, such as safety and sustainability, in nuclear applications. HEAs consisting of refractory elements naturally have high transmutation resistance, low affinity for neutron capture and reduced activation characteristics [243]. Some of the RHEAs, having single-phase BCC structures, i.e., MoNbTaTi, MoNbTaTiW, and WTaCrVHf, were designed and manufactured to resist the irradiation occurring in nuclear plants [244,245]. Recently, Moschetti et al. proposed a method to compare and determine the most suitable HEA candidates for advanced nuclear applications considering the available nuclear data. Findings revealed that $Al_{20}Be_{20}Fe_{10}Si_{15}Ti_{35}$ and $V_{35}Ti_{35}Fe_{15}Cr_{10}Zr_5$ alloys have long decay times under gamma dose and the HEAs developed based on AlBeFeSiTi system have promising neutron irradiation resistance although their performance was not fully investigated yet [243].

8. Challenges and future perspectives

AM-ed HEAs have great potential as replacements for existing engineering materials due to their outstanding properties. A high degree of freedom in alloy design, using physical metallurgy principles, CALPHAD-based thermodynamics calculations, or data-driven approaches, allows us to overcome the limitations faced by previously developed HEAs. The advances in AM techniques and their extensive acceptance into mainstream manufacturing routes also help to overcome existing limitations. Therefore, AM can greatly facilitate the exploration of the vast HEA universe and advance research in this area. Nevertheless, some challenges have been identified and some future perspectives can be envisioned for the next-step development from this review:

[1] The number and type of AM-ed HEAs have been limited by specific requirements on the quality of the feedstock and complexity in the solidification behavior. Although CoCrFeNi-based HEAs produced by AM were first reported back in 2015, the alloy development has been rather slow. The printability and performance of novel HEAs should continue to be investigated using promising AM techniques. The production of magnetic, lightweight, or refractory HEAs via PBF techniques remain challenging due to the susceptibility to cracking and porosity and alloy complexity, although the rapid developments in AM and powder metallurgy techniques hold great promise to overcome these challenges in the coming years considering the design freedom and unexplored potentials of processing control via AM.

[2] Previous studies have demonstrated that the feedstock can be modified via *in situ* or *ex situ* alloying methods to have a greater freedom in alloy design. For example, these modifications can be applied to DED and WAAM-based techniques by altering the composition for each layer or simultaneously using multiple powder or wire feedstocks. Using process control to realize compositional control is certainly a great challenge, but this possibility brings unique advantages to create HEA matrix composites and functionally graded HEAs and may accelerate the acceptance of AM techniques into the materials development cycle.

[3] Alloy development by trial-and-error is both time and material-consuming, and novel approaches are urgently needed. High-throughput screening via data-driven methods can accelerate alloy development and enhance sustainability. Advances in machine learning or artificial intelligence will further be implemented into the alloy development process; thus, researchers should be encouraged to share their data to generate a complete database including medium-/high-entropy alloys with their corresponding manufacturing methods.

[4] The genuine capabilities of AM can be demonstrated by manufacturing complex geometries [246–248], although conceptual structures have been manufactured in a few studies. Solidification behavior with complex geometries should then be evaluated to pave the way for adapting AM technologies to mainstream manufacturing, and eventually replacing conventionally produced counterparts with AM-ed HEAs. These complex geometries and the resultant variation in the thermal history of

AM-ed HEAs, should be carefully designed and analyzed, particularly for multi-phase HEAs.

[5] The AM processes still require further optimizations to enhance the performance of HEAs by tailoring the microstructures, for example avoiding phase separation by lowering the pre-heating temperature or modifying the alloy stoichiometry. Post-process treatments should also be employed, where necessary, to modify and/or to stabilize the microstructure of AM-ed HEAs, to eliminate the process-related defects and to achieve superior mechanical properties [205,249,250]. Recent adaptations of *in situ* process monitoring in additive manufacturing techniques will further be employed in assessing the process-structure relationship while allowing accelerated process optimization based on users' need.

[6] Most current studies explored the structural properties of AM-ed HEAs by investigating their hardness and compressive and tensile strength; properties such as fatigue life and fracture toughness are, however, less investigated. Their functional properties, such as magnetic properties, hydrogen storage capacity, and wear and corrosion resistance, also remain to be discovered. The alloy design for AM-ed HEAs should also be functionality-oriented if they are intended for functional materials. The versatility of surface characteristics of AM-ed HEAs might help maximize the functionality of these alloys as compared to the ones manufactured be employing conventional routes.

[7] The room-temperature, or even cryogenic properties of AM-ed single-phase HEAs, such as CoCrFeMnNi, have been reported in numerous studies; however, their high-temperature performance has not been explored. Analyses of LPBF-built CoCrFeMnNi HEA at high temperatures have been limited to hardness and compressive strength [251]. However, high-density dislocations, the main contributor to the high strength of LPBF-built CoCrFeMnNi HEAs at room temperature, may annihilate at elevated temperatures [252]. Investigating the phase stability and the resulting mechanical performance of AM-ed HEAs at high temperatures is thus necessary to evaluate their application potential in high-temperature environments.

9. Conclusions

The state-of-the-art of AM-ed HEAs was extensively reviewed in terms of alloy development, printability using various feedstocks, potential manufacturing defects, AM techniques, and the microstructure-property relationship. The most significant characteristics, advantages, disadvantages, and applications of AM techniques regarding manufacturing single- or multi-phase HEAs are summarized in Table 4. It presents a helpful framework for researchers working with HEAs, facilitating the informed selection of AM techniques and supporting the development of novel HEA compositions.

AM exhibits great potential in providing promising materials with the desired microstructure and mechanical properties as it has been reviewed in this paper. However, the complexity of solidification and remelting during AM brings new challenges to materials design. The choice of feedstocks plays an important role on maintaining the chemical homogeneity. Gas and plasma atomization methods are commonly used to produce high-quality powder feedstocks, although *in situ* and *ex situ* alloying techniques offer cost-effective alternatives. Various upgrades/apparatus attached to existing LPBF, DED, and BJP systems also enable the development of functionally graded HEAs or HEA matrix composites via *in situ* and *ex situ* alloying techniques.

Microstructural evolution during AM was mainly classified into two main categories—single-phase and multi-phase HEAs, including EHEAs and ODS-HEAs,—to show its effect on the mechanical performance of AM-ed HEAs. Single-phase HEAs, with FCC, BCC, or HCP structures, have a relatively consistent performance at cryogenic, room, and elevated temperatures, compared to that in multi-phase HEAs. In multi-phase HEAs, secondary phases like carbides and nitrides, together with segregations, greatly increased hardness and strength, but their distributions around grain and cellular boundaries tend to deteriorate ductility of as-built alloys. In general, higher cooling rates, a unique

Table 4
Summary of AM techniques employed to manufacture HEAs.

AM Technique	Solidification Rate	Chemical Homogeneity	Dislocation Cell Size	Dislocation Density	Texture Type	Microstructure of as-built HEAs	Advantages	Disadvantages	Applications in HEAs
LPBF	Very High	Might have localized segregation due to rapid solidification	Smaller cell size	Very high	Preferential texture along build direction	Fine-grained microstructures, tailorable grain size and orientation	High accuracy, resolution, wide material compatibility, complex geometries, strong parts	Limited build volume, slow build speed, requires post-processing depending on alloys	High-performance components, turbine blades, heat exchangers, biomedical implants
EPBF	High	Might have localized segregation due to rapid solidification	Slightly coarser than LPBF	High	Preferential texture along build direction	Fine microstructures (coarser than LPBF)	Faster build speed, larger build volume, vacuum environment high preheating temperature, higher melting temperatures	Higher cost than LPBF, limited material compatibility	Large-scale components, biomedical implants, tools and dies, wear-resistant parts
DED	Moderate to high	Less homogeneity than LPBF/ EPBF due to localized high energy input	Cell size varies across the build	Moderate to high	Texture following thermal gradients	Variable microstructures within the same build (thermal gradients), *in situ* heat treatment opportunity	Flexible, adaptable, build on existing parts, high deposition rate	Lower accuracy, higher surface roughness than PBF, requires careful process control	Repair and cladding, AM of large structures, composites
BJP	Low	Good homogeneity after sintering	NA	NA	Tailorable texture through post-process heat treatment	Infiltration with different alloy can result in multi-phase HEAs	Low cost, high build speed, wide range of materials	Lower part strength and density, limited resolution, requires post-processing	Porous structures, lightweight components, rapid prototyping

advantage of AM techniques, trigger grain refinement and contribute to strengthening via introducing more dislocations in HEAs in as-built materials. Notably, HEAs produced by DED, LPBF, and BJP typically show better mechanical performance than those produced by EPBF, due to better grain refinement. Additionally, DED or LPBF has the versatility of being able to fine-tune the microstructure, such as grain size, morphology, and texture, to modify the mechanical properties of both single and multi-phase HEAs considering approach-based process design and optimization.

Despite the significant progress, several challenges remain. The key challenge across various AM techniques lies in achieving precise microstructural control. Achieving consistent chemical homogeneity, controlling the formation of undesirable phases, and mitigating defects such as porosity and cracking are also other ongoing issues that need to be addressed. To unlock the full application potential of AM-ed HEAs as both functional and structural materials, a strategic approach should be taken, incorporating process optimization and enhanced materials design. Thus, the review suggests that further research and development in process optimization, advanced materials design, and real-time monitoring of the AM process are essential to overcoming these challenges.

CRediT authorship contribution statement

Mehmet Cagirici: Writing – original draft, Writing – review & editing, Visualization, Investigation, Formal analysis, Data curation. **Sheng Guo:** Writing – review & editing, Resources, Formal analysis. **Jun Ding:** Writing – review & editing, Validation, Supervision. **Upadrasta Ramamurty:** Writing – review & editing, Supervision, Resources. **Pan Wang:** Writing – original draft, Writing – review & editing, Visualization, Investigation, Formal analysis, Data curation, Supervision, Resources, Project administration, Conceptualization.

Declaration of competing interest

The authors declare that they have no known competing financial interests or personal relationships that could have appeared to influence the work reported in this paper.

One of the co-authors, Wang Pan, as an Editorial Board Member of 'Smart Materials in Manufacturing,' was not involved in the editorial review or the decision to publish this article and had no access to information regarding its review process.

References

[1] E.E. Herderick, Additive Manufacturing of Metals: A Review, Materials Science and Technology (MS&T), 2011, pp. 1413–1425. Columbus, OH.
[2] W.E. Frazier, Metal additive manufacturing: a review, J. Mater. Eng. Perform. 23 (6) (2014) 1917–1928.
[3] D. Herzog, V. Seyda, E. Wycisk, C. Emmelmann, Additive manufacturing of metals, Acta Mater. 117 (2016) 371–392.
[4] Y. Kok, X.P. Tan, P. Wang, M.L.S. Nai, N.H. Loh, E. Liu, S.B. Tor, Anisotropy and heterogeneity of microstructure and mechanical properties in metal additive manufacturing: a critical review, Mater. Des. 139 (2018) 565–586.
[5] B. Cantor, I.T.H. Chang, P. Knight, A.J.B. Vincent, Microstructural development in equiatomic multicomponent alloys, Mater. Sci. Eng., A 375–377 (2004) 213–218.
[6] K.H. Huang, J.W. Yeh, A Study on Multicomponent Alloy Systems Containing Equal-Mole Elements, National Tsing Hua University, 1996.
[7] J.W. Yeh, S.K. Chen, S.J. Lin, J.Y. Gan, T.S. Chin, T.T. Shun, C.H. Tsau, S. Y. Chang, Nanostructured high-entropy alloys with multiple principal elements: novel alloy design concepts and outcomes, Adv. Eng. Mater. 6 (5) (2004) 299–303.
[8] J. Joseph, N. Stanford, P. Hodgson, D.M. Fabijanic, Tension/compression asymmetry in additive manufactured face centered cubic high entropy alloy, Scripta Mater. 129 (2017) 30–34.
[9] J. Guo, M. Goh, Z. Zhu, X. Lee, M.L.S. Nai, J. Wei, On the machining of selective laser melting CoCrFeMnNi high-entropy alloy, Mater. Des. 153 (2018) 211–220.
[10] F. Peyrouzet, D. Hachet, R. Soulas, C. Navone, S. Godet, S. Gorsse, Selective laser melting of Al0.3CoCrFeNi high-entropy alloy: printability, microstructure, and mechanical properties, J. Miner. Met. Mater. Soc. 71 (10) (2019) 3443–3451.
[11] B. Gwalani, V. Soni, O.A. Waseem, S.A. Mantri, R. Banerjee, Laser additive manufacturing of compositionally graded AlCrFeMoVx (x = 0 to 1) high-entropy alloy system, Opt Laser. Technol. 113 (2019) 330–337.
[12] Y.J. Zhao, J.W. Qiao, S.G. Ma, M.C. Gao, H.J. Yang, M.W. Chen, Y. Zhang, A hexagonal close-packed high-entropy alloy: the effect of entropy, Mater. Des. 96 (2016) 10–15.
[13] B. Gludovatz, A. Hohenwarter, D. Catoor, E.H. Chang, E.P. George, R.O. Ritchie, A fracture-resistant high-entropy alloy for cryogenic applications, Science 345 (6201) (2014) 1153–1158.
[14] Z. Qiu, C. Yao, K. Feng, Z. Li, P.K. Chu, Cryogenic deformation mechanism of CrMnFeCoNi high-entropy alloy fabricated by laser additive manufacturing process, Int. J. Lightweight Mater. Manufact 1 (1) (2018) 33–39.
[15] W.-R. Wang, W.-L. Wang, J.-W. Yeh, Phases, microstructure and mechanical properties of AlxCoCrFeNi high-entropy alloys at elevated temperatures, J. Alloys Compd. 589 (2014) 143–152.
[16] T. Fujieda, H. Shiratori, K. Kuwabara, T. Kato, K. Yamanaka, Y. Koizumi, A. Chiba, First demonstration of promising selective electron beam melting method for utilizing high-entropy alloys as engineering materials, Mater. Lett. 159 (2015) 12–15.
[17] Y.S. Kim, H. Chae, W. Woo, D.-K. Kim, D.-H. Lee, S. Harjo, T. Kawasaki, S.Y. Lee, Multiple deformation scheme in direct energy deposited CoCrNi medium entropy alloy at 210K, Mater. Sci. Eng., A 828 (2021) 142059.
[18] H.G. Li, Y.J. Huang, W.J. Zhao, T. Chen, J.F. Sun, D.Q. Wei, Q. Du, Y.C. Zou, Y. Z. Lu, P. Zhu, X. Lu, A.H.W. Ngan, Overcoming the strength-ductility trade-off in an additively manufactured CoCrFeMnNi high entropy alloy via deep cryogenic treatment, Addit. Manuf. 50 (2022) 102546.
[19] G. Laplanche, U.F. Volkert, G. Eggeler, E.P. George, Oxidation behavior of the CrMnFeCoNi high-entropy alloy, Oxid. Metals 85 (5) (2016) 629–645.
[20] T. Fujieda, H. Shiratori, K. Kuwabara, M. Hirota, T. Kato, K. Yamanaka, Y. Koizumi, A. Chiba, S. Watanabe, CoCrFeNiTi-based high-entropy alloy with superior tensile strength and corrosion resistance achieved by a combination of additive manufacturing using selective electron beam melting and solution treatment, Mater. Lett. 189 (2017) 148–151.
[21] M.A. Melia, J.D. Carroll, S.R. Whetten, S.N. Esmaeely, J. Locke, E. White, I. Anderson, M. Chandross, J.R. Michael, N. Argibay, E.J. Schindelholz, A. B. Kustas, Mechanical and corrosion properties of additively manufactured CoCrFeMnNi high entropy alloy, Addit. Manuf. 29 (2019) 100833.
[22] S. Xia, Z. Xia, D. Zhao, Y. Xie, X. Liu, L. Wang, Microstructure formation mechanism and corrosion behavior of FeCrCuTiV two-phase high entropy alloy prepared by different processes, Fusion Eng. Des. 172 (2021) 112792.
[23] X. Qiu, Microstructure and corrosion properties of Al2CrFeCoxCuNiTi high entropy alloys prepared by additive manufacturing, J. Alloys Compd. 887 (2021) 161422.
[24] P. Chen, C. Lee, S.-Y. Wang, M. Seifi, J.J. Lewandowski, K.A. Dahmen, H. Jia, X. Xie, B. Chen, J.-W. Yeh, C.-W. Tsai, T. Yuan, P.K. Liaw, Fatigue behavior of high-entropy alloys: a review, Sci. China Technol. Sci. 61 (2) (2018) 168–178.
[25] S. Shukla, T. Wang, S. Cotton, R.S. Mishra, Hierarchical microstructure for improved fatigue properties in a eutectic high entropy alloy, Scripta Mater. 156 (2018) 105–109.
[26] Z. Tang, T. Yuan, C.-W. Tsai, J.-W. Yeh, C.D. Lundin, P.K. Liaw, Fatigue behavior of a wrought Al0.5CoCrCuFeNi two-phase high-entropy alloy, Acta Mater. 99 (2015) 247–258.
[27] M. Bönisch, Y. Wu, H. Sehitoglu, Twinning-induced strain hardening in dual-phase FeCoCrNiAl0.5 at room and cryogenic temperature, Sci. Rep. 8 (1) (2018) 10663.
[28] Y. Deng, C.C. Tasan, K.G. Pradeep, H. Springer, A. Kostka, D. Raabe, Design of a twinning-induced plasticity high entropy alloy, Acta Mater. 94 (2015) 124–133.
[29] Z. Yang, D. Yan, W. Lu, Z. Li, A TWIP-TRIP quinary high-entropy alloy: tuning phase stability and microstructure for enhanced mechanical properties, Mater. Sci. Eng., A 801 (2021) 140441.
[30] Z. Li, C.C. Tasan, K.G. Pradeep, D. Raabe, A TRIP-assisted dual-phase high-entropy alloy: grain size and phase fraction effects on deformation behavior, Acta Mater. 131 (2017) 323–335.
[31] J. Li, Q. Fang, B. Liu, Y. Liu, Transformation induced softening and plasticity in high entropy alloys, Acta Mater. 147 (2018) 35–41.
[32] Y.H. Jo, S. Jung, W.M. Choi, S.S. Sohn, H.S. Kim, B.J. Lee, N.J. Kim, S. Lee, Cryogenic strength improvement by utilizing room-temperature deformation twinning in a partially recrystallized VCrMnFeCoNi high-entropy alloy, Nat. Commun. 8 (2017) 15719.
[33] M. Hörnqvist Colliander, D. Haase, K. Glazyrin, A. Edgren, P. Wang, M. Guthrie, S. Guo, Cryogenic temperatures promote the pressure-induced polymorphic transition in CoCrFeMnNi high entropy alloy, J. Appl. Phys. 136 (11) (2024).
[34] Z. He, N. Jia, H. Wang, H. Yan, Y. Shen, Synergy effect of multi-strengthening mechanisms in FeMnCoCrN HEA at cryogenic temperature, J. Mater. Sci. Technol. 86 (2021) 158–170.
[35] Y.H. Jo, W.M. Choi, D.G. Kim, A. Zargaran, S.S. Sohn, H.S. Kim, B.J. Lee, N. J. Kim, S. Lee, FCC to BCC transformation-induced plasticity based on thermodynamic phase stability in novel V10Cr10Fe45CoxNi35−x medium-entropy alloys, Sci. Rep. 9 (1) (2019) 2948.
[36] J. Yang, Y.H. Jo, D.W. Kim, W.-M. Choi, H.S. Kim, B.-J. Lee, S.S. Sohn, S. Lee, Effects of transformation-induced plasticity (TRIP) on tensile property improvement of Fe45Co30Cr10V10Ni5-xMnx high-entropy alloys, Mater. Sci. Eng., A 772 (2020) 138809.
[37] L. Zhao, L. Jiang, L.X. Yang, H. Wang, W.Y. Zhang, G.Y. Ji, X. Zhou, W.A. Curtin, X.B. Chen, P.K. Liaw, S.Y. Chen, H.Z. Wang, High throughput synthesis enabled

exploration of CoCrFeNi-based high entropy alloys, J. Mater. Sci. Technol. 110 (2022) 269–282.
[38] Y. Zhang, Q. Xing, High entropy alloys: manufacturing routes, in: F.G. Caballero (Ed.), Encyclopedia of Materials: Metals and Alloys, Elsevier, Oxford, 2022, pp. 327–338.
[39] K. Zhou, J. Li, Q. Wu, Z. Zhang, Z. Wang, J. Wang, Remelting induced fully-equiaxed microstructures with anomalous eutectics in the additive manufactured Ni32Co30Cr10Fe10Al18 eutectic high-entropy alloy, Scripta Mater. 201 (2021) 113952.
[40] V. Gromov, Y. Ivanov, S. Konovalov, K. Osintsev, A. Semin, Y. Rubannikova, Modification of high-entropy alloy AlCoCrFeNi by electron beam treatment, J. Mater. Res. Technol. 13 (2021) 787–797.
[41] M. Valizadeh, S.J. Wolff, Convolutional Neural Network applications in additive manufacturing: a review, Adv. Indust. Manufacturing Eng. (2022) 100072.
[42] T. Nagase, M. Todai, P. Wang, S.-H. Sun, T. Nakano, Design and development of (Ti, Zr, Hf)-Al based medium entropy alloys and high entropy alloys, Mater. Chem. Phys. 276 (2022).
[43] Y. Iijima, T. Nagase, A. Matsugaki, P. Wang, K. Ameyama, T. Nakano, Design and development of Ti–Zr–Hf–Nb–Ta–Mo high-entropy alloys for metallic biomaterials, Mater. Des. 202 (2021).
[44] Y. Brif, M. Thomas, I. Todd, The use of high-entropy alloys in additive manufacturing, Scripta Mater. 99 (2015) 93–96.
[45] S. Chen, Y. Tong, P. Liaw, Additive manufacturing of high-entropy alloys: a review, Entropy 20 (12) (2018) 937.
[46] O.N. Senkov, D.B. Miracle, K.J. Chaput, J.-P. Couzinie, Development and exploration of refractory high entropy alloys—a review, J. Mater. Res. 33 (19) (2018) 3092–3128.
[47] J. Joseph, T. Jarvis, X. Wu, N. Stanford, P. Hodgson, D.M. Fabijanic, Comparative study of the microstructures and mechanical properties of direct laser fabricated and arc-melted AlxCoCrFeNi high entropy alloys, Mater. Sci. Eng., A 633 (2015) 184–193.
[48] V. Ocelík, N. Janssen, S.N. Smith, J.T.M. De Hosson, Additive manufacturing of high-entropy alloys by laser processing, J. Miner. Met. Mater. Soc. 68 (7) (2016) 1810–1818.
[49] Q. Sui, Z. Wang, J. Wang, S. Xu, F. Zhao, L. Gong, B. Liu, J. Liu, G. Liu, The microstructure and mechanical properties of the additive manufactured AlCoCrFeNi high entropy alloy, Mater. Sci. Eng., A 833 (2022) 142507.
[50] A. Ostovari Moghaddam, N.A. Shaburova, M.N. Samodurova, A. Abdollahzadeh, E.A. Trofimov, Additive manufacturing of high entropy alloys: a practical review, J. Mater. Sci. Technol. 77 (2021) 131–162.
[51] Y. Cai, L. Zhu, Y. Cui, J. Han, Manufacturing of FeCoCrNi + FeCoCrNiAl laminated high-entropy alloy by laser melting deposition (LMD), Mater. Lett. 289 (2021) 129445.
[52] Y. Zhao, K.B. Lau, W.H. Teh, J.J. Lee, F. Wei, M. Lin, P. Wang, C.C. Tan, U. Ramamurty, Compositionally graded CoCrFeNiTix high-entropy alloys manufactured by laser powder bed fusion: a combinatorial assessment, J. Alloys Compd. 883 (2021) 160825.
[53] B. Dong, Z. Wang, Z. Pan, O. Muránsky, C. Shen, M. Reid, B. Wu, X. Chen, H. Li, On the development of pseudo-eutectic AlCoCrFeNi2.1 high entropy alloy using Powder-bed Arc Additive Manufacturing (PAAM) process, Mater. Sci. Eng., A 802 (2021) 140639.
[54] W. Zhao, J.-K. Han, Y.O. Kuzminova, S.A. Evlashin, A.P. Zhilyaev, A.M. Pesin, J.-i. Jang, K.-D. Liss, M. Kawasaki, Significance of grain refinement on micro-mechanical properties and structures of additively-manufactured CoCrFeNi high-entropy alloy, Mater. Sci. Eng., A 807 (2021) 140898.
[55] H. Li, Y. Huang, S. Jiang, Y. Lu, X. Gao, X. Lu, Z. Ning, J. Sun, Columnar to equiaxed transition in additively manufactured CoCrFeMnNi high entropy alloy, Mater. Des. 197 (2021) 109262.
[56] H. Zhang, Y. Zhao, J. Cai, S. Ji, J. Geng, X. Sun, D. Li, High-strength NbMoTaX refractory high-entropy alloy with low stacking fault energy eutectic phase via laser additive manufacturing, Mater. Des. 201 (2021) 109462.
[57] W. Zhang, A. Chabok, B.J. Kooi, Y. Pei, Additive manufactured high entropy alloys: a review of the microstructure and properties, Mater. Des. 220 (2022) 110875.
[58] P. Sreeramagiri, G. Balasubramanian, Directed energy deposition of multi-principal element alloys, Front. Mater. 9 (2022).
[59] P. Sathiyamoorthi, H.S. Kim, High-entropy alloys with heterogeneous microstructure: processing and mechanical properties, Prog. Mater. Sci. 123 (2022) 100709.
[60] Z. Liu, D. Zhao, P. Wang, M. Yan, C. Yang, Z. Chen, J. Lu, Z. Lu, Additive manufacturing of metals: microstructure evolution and multistage control, J. Mater. Sci. Technol. 100 (2022) 224–236.
[61] J. Kim, A. Wakai, A. Moridi, Materials and manufacturing renaissance: additive manufacturing of high-entropy alloys, J. Mater. Res. 35 (15) (2020) 1963–1983.
[62] E.P. George, W.A. Curtin, C.C. Tasan, High entropy alloys: a focused review of mechanical properties and deformation mechanisms, Acta Mater. 188 (2020) 435–474.
[63] E.P. George, D. Raabe, R.O. Ritchie, High-entropy alloys, Nat. Rev. Mater. 4 (8) (2019) 515–534.
[64] ASTM, Standard Terminology for Additive Manufacturing Technologies, ASTM International, West Conshohocken, PA, 2010. ASTM F2792-12a.
[65] ASTM, Additive Manufacturing — General Principles — Fundamentals and Vocabulary, ASTM International, 2021.
[66] E. Davoodi, H. Montazerian, A.S. Mirhakimi, M. Zhianmanesh, O. Ibhadode, S. I. Shahabad, R. Esmaeilizadeh, E. Sarikhani, S. Toorandaz, S.A. Sarabi, R. Nasiri, Y. Zhu, J. Kadkhodapour, B. Li, A. Khademhosseini, E. Toyserkani, Additively manufactured metallic biomaterials, Bioact. Mater. 15 (2022) 214–249.
[67] T. Fujieda, M. Chen, H. Shiratori, K. Kuwabara, K. Yamanaka, Y. Koizumi, A. Chiba, S. Watanabe, Mechanical and corrosion properties of CoCrFeNiTi-based high-entropy alloy additive manufactured using selective laser melting, Addit. Manuf. 25 (2019) 412–420.
[68] M. Zhang, X. Zhou, D. Wang, W. Zhu, J. Li, Y.F. Zhao, AlCoCuFeNi high-entropy alloy with tailored microstructure and outstanding compressive properties fabricated via selective laser melting with heat treatment, Mater. Sci. Eng., A 743 (2019) 773–784.
[69] Z. Sun, X.P. Tan, M. Descoins, D. Mangelinck, S.B. Tor, C.S. Lim, Revealing hot tearing mechanism for an additively manufactured high-entropy alloy via selective laser melting, Scripta Mater. 168 (2019) 129–133.
[70] P. Wang, P. Huang, F.L. Ng, W.J. Sin, S. Lu, M.L.S. Nai, Z. Dong, J. Wei, Additively manufactured CoCrFeNiMn high-entropy alloy via pre-alloyed powder, Mater. Des. 168 (2019).
[71] M. Cagirici, P. Wang, F.L. Ng, M.L.S. Nai, J. Ding, J. Wei, Additive manufacturing of high-entropy alloys by thermophysical calculations and in situ alloying, J. Mater. Sci. Technol. 94 (2021) 53–66.
[72] Y.-K. Kim, K.-A. Lee, Stabilized sub–grain and nano carbides–driven 1.2GPa grade ultra–strong CrMnFeCoNi high–entropy alloy additively manufactured by laser powder bed fusion, J. Mater. Sci. Technol. 117 (2022) 8–22.
[73] Q. Jiang, P. Zhang, Z. Yu, Y. Tian, S. Ma, AlCoCrFeNi high entropy alloy fabricated via selective laser melting reinforced by Fe-based metallic glass, Mater. Lett. 307 (2022) 130994.
[74] L. He, S. Wu, A. Dong, H. Tang, D. Du, G. Zhu, B. Sun, W. Yan, Selective laser melting of dense and crack-free AlCoCrFeNi2.1 eutectic high entropy alloy: synergizing strength and ductility, J. Mater. Sci. Technol. 117 (2022) 133–145.
[75] M. Zhang, X. Zhou, D. Wang, L. He, X. Ye, W. Zhang, Additive manufacturing of in-situ strengthened dual-phase AlCoCuFeNi high-entropy alloy by selective electron beam melting, J. Alloys Compd. 893 (2022) 162259.
[76] W.J. Sames, F.A. List, S. Pannala, R.R. Dehoff, S.S. Babu, The metallurgy and processing science of metal additive manufacturing, Int. Mater. Rev. 61 (5) (2016) 315–360.
[77] P.K. Gokuldoss, S. Kolla, J. Eckert, Additive manufacturing processes: selective laser melting, electron beam melting and binder jetting—selection guidelines, Materials 10 (6) (2017) 672.
[78] X. Li, Y.H. Tan, P. Wang, X. Su, H.J. Willy, T.S. Herng, J. Ding, Metallic microlattice and epoxy interpenetrating phase composites: experimental and simulation studies on superior mechanical properties and their mechanisms, Compos. Appl. Sci. Manuf. 135 (2020) 105934.
[79] P. Wang, X. Li, Y. Jiang, M.L.S. Nai, J. Ding, J. Wei, Electron beam melted heterogeneously porous microlattices for metallic bone applications: design and investigations of boundary and edge effects, Addit. Manuf. 36 (2020).
[80] P. Wang, X. Li, S. Luo, M.L.S. Nai, J. Ding, J. Wei, Additively manufactured heterogeneously porous metallic bone with biostructural functions and bone-like mechanical properties, J. Mater. Sci. Technol. 62 (2021) 173–179.
[81] P. Wang, X. Tan, M.L.S. Nai, J. Wu, J. Wei, Deformation induced nanoscale twinning improves strength and ductility in additively manufactured titanium alloys, Mater. Sci. Eng., A 833 (2022) 142568.
[82] P. Wang, M.L.S. Nai, W.J. Sin, S. Lu, B. Zhang, J. Bai, J. Song, J. Wei, Realizing a full volume component by in-situ welding during electron beam melting process, Addit. Manuf. 22 (2018) 375–380.
[83] H. Amano, T. Ishimoto, K. Hagihara, R. Suganuma, K. Aiba, S.-H. Sun, P. Wang, T. Nakano, Impact of gas flow direction on the crystallographic texture evolution in laser beam powder bed fusion, Virtual, Phys. Prototyp. 18 (1) (2023).
[84] W. Zhai, P. Wang, F.L. Ng, W. Zhou, S.M. Ling Nai, J. Wei, Hybrid manufacturing of γ-TiAl and Ti–6Al–4V bimetal component with enhanced strength using electron beam melting, Compos. B Eng. (2020) 108587.
[85] A. Dass, A. Moridi, State of the art in directed energy deposition: from additive manufacturing to materials design, Coatings 9 (7) (2019) 418.
[86] D. Svetlizky, M. Das, B. Zheng, A.L. Vyatskikh, S. Bose, A. Bandyopadhyay, J. M. Schoenung, E.J. Lavernia, N. Eliaz, Directed energy deposition (DED) additive manufacturing: physical characteristics, defects, challenges and applications, Mater. Today 49 (2021) 271–295.
[87] S. Xiang, J. Li, H. Luan, A. Amar, S. Lu, K. Li, L. Zhang, X. Liu, G. Le, X. Wang, F. Qu, W. Zhang, D. Wang, Q. Li, Effects of process parameters on microstructures and tensile properties of laser melting deposited CrMnFeCoNi high entropy alloys, Mater. Sci. Eng., A 743 (2019) 412–417.
[88] H. Dobbelstein, E.L. Gurevich, E.P. George, A. Ostendorf, G. Laplanche, Laser metal deposition of a refractory TiZrNbHfTa high-entropy alloy, Addit. Manuf. 24 (2018) 386–390.
[89] I. Kunce, M. Polanski, K. Karczewski, T. Plocinski, K.J. Kurzydlowski, Microstructural characterisation of high-entropy alloy AlCoCrFeNi fabricated by laser engineered net shaping, J. Alloys Compd. 648 (2015) 751–758.
[90] Y. Cai, X. Li, H. Xia, Y. Cui, S.M. Manladan, L. Zhu, M. Shan, D. Sun, T. Wang, X. Lv, J. Han, Fabrication of laminated high entropy alloys using differences in laser melting deposition characteristics of FeCoCrNi and FeCoCrNiAl, J. Manuf. Process. 72 (2021) 294–308.
[91] T. Nguyen, M. Huang, H. Li, V. Tran, S. Yang, Microstructure and tensile properties of duplex phase Al0.25FeMnNiCrCu0.5 high entropy alloy fabricated by laser melting deposition, J. Alloys Compd. 871 (2021) 159521.
[92] Q. Shen, X. Kong, X. Chen, Significant transitions of microstructure and mechanical properties in additively manufactured Al–Co–Cr–Fe–Ni high-entropy alloy under heat treatment, Mater. Sci. Eng., A 815 (2021) 141257.

[93] M.R.U. Ahsan, G.-J. Seo, X. Fan, P.K. Liaw, S. Motaman, C. Haase, D.B. Kim, Effects of process parameters on bead shape, microstructure, and mechanical properties in wire + arc additive manufacturing of Al0.1CoCrFeNi high-entropy alloy, J. Manuf. Process. 68 (2021) 1314–1327.
[94] Q. Shen, X. Kong, X. Chen, Fabrication of bulk Al-Co-Cr-Fe-Ni high-entropy alloy using combined cable wire arc additive manufacturing (CCW-AAM): microstructure and mechanical properties, J. Mater. Sci. Technol. 74 (2021) 136–142.
[95] K. Osintsev, S. Konovalov, D. Zaguliaev, Y. Ivanov, V. Gromov, I. Panchenko, Investigation of Co-Cr-Fe-Mn-Ni non-equiatomic high-entropy alloy fabricated by wire arc additive manufacturing, Metals 12 (2) (2022) 197.
[96] M. Sachs Emanuel, S. Haggerty John, J. Cima Michael, A. Williams Paul, Three-dimensional Printing Techniques, MASSACHUSETTS INST TECHNOLOGY, US, 1993.
[97] M. Zenou, L. Grainger, Additive manufacturing of metallic materials, in: J. Zhang, Y.-G. Jung (Eds.), Addit. Manuf., Butterworth-Heinemann, 2018, pp. 53–103.
[98] M. Turker, D. Godlinski, F. Petzoldt, Effect of production parameters on the properties of IN 718 superalloy by three-dimensional printing, Mater. Char. 59 (12) (2008) 1728–1735.
[99] D. Karlsson, G. Lindwall, A. Lundbäck, M. Amnebrink, M. Boström, L. Riekehr, M. Schuisky, M. Sahlberg, U. Jansson, Binder jetting of the AlCoCrFeNi alloy, Addit. Manuf. 27 (2019) 72–79.
[100] N.D. Parab, J.E. Barnes, C. Zhao, R.W. Cunningham, K. Fezzaa, A.D. Rollett, T. Sun, Real time observation of binder jetting printing process using high-speed X-ray imaging, Sci. Rep. 9 (1) (2019) 2499.
[101] Z. Xu, Z. Zhu, P. Wang, G.K. Meenashisundaram, S.M.L. Nai, J. Wei, Fabrication of porous CoCrFeMnNi high entropy alloy using binder jetting additive manufacturing, Addi, Manuf. 35 (2020) 101441.
[102] O. Gokcekaya, T. Ishimoto, T. Todo, P. Wang, T. Nakano, Influence of powder characteristics on densification via crystallographic texture formation: pure tungsten prepared by laser powder bed fusion, Additive Manufacturing Letters 1 (2021).
[103] P. Wang, M.L.S. Nai, F.L. Ng, A. Tan, W.J. Sin, M.H. Goh, Y. Maruno, Revealing mechanisms underlying powder reusability of Ti-48Al-2Cr-2Nb intermetallic in electron beam powder bed fusion process, Addit. Manuf. 59 (2022).
[104] S. Ziri, A. Hor, C. Mabru, Combined effect of powder properties and process parameters on the density of 316L stainless steel obtained by laser powder bed fusion, Int. J. Adv. Des. Manuf. Technol. 120 (9) (2022) 6187–6204.
[105] S. Ghods, R. Schur, E. Schultz, R. Pahuja, A. Montelione, C. Wisdom, D. Arola, M. Ramulu, Powder reuse and its contribution to porosity in additive manufacturing of Ti6Al4V, Materialia 15 (2021) 100992.
[106] K. Joshi, P. Promoppatum, S.S. Quek, S. Raghavan, N.S. Johan, S. Shukla, S. Samudrala, S. van der Veen, M.H. Jhon, Effect of porosity distribution on the strength and strain-to-failure of Laser-Powder Bed Fusion printed Ti–6Al–4V, Addit. Manuf. 75 (2023) 103738.
[107] L. Xiong, A.C. Chuang, J. Thomas, T. Prost, E. White, I. Anderson, D. Singh, Defect and satellite characteristics of additive manufacturing metal powders, Adv. Powder Technol. 33 (3) (2022) 103486.
[108] A. Mussatto, R. Groarke, A. O'Neill, M.A. Obeidi, Y. Delaure, D. Brabazon, Influences of powder morphology and spreading parameters on the powder bed topography uniformity in powder bed fusion metal additive manufacturing, Addit. Manuf. 38 (2021) 101807.
[109] J. Dawes, R. Bowerman, R. Trepleton, Introduction to the additive manufacturing powder metallurgy supply chain, Johnson Matthey Technol. Rev. 59 (3) (2015) 243–256.
[110] Z.G. Zhu, Q.B. Nguyen, F.L. Ng, X.H. An, X.Z. Liao, P.K. Liaw, S.M.L. Nai, J. Wei, Hierarchical microstructure and strengthening mechanisms of a CoCrFeNiMn high entropy alloy additively manufactured by selective laser melting, Scripta Mater. 154 (2018) 20–24.
[111] I.E. Anderson, E.M.H. White, R. Dehoff, Feedstock powder processing research needs for additive manufacturing development, Curr. Opin. Solid State Mater. Sci. 22 (1) (2018) 8–15.
[112] S. Ewald, F. Kies, S. Hermsen, M. Voshage, C. Haase, J.H. Schleifenbaum, Rapid alloy development of extremely high-alloyed metals using powder blends in laser powder bed fusion, Materials 12 (10) (2019) 1706.
[113] B. Li, L. Zhang, Y. Xu, Z. Liu, B. Qian, F. Xuan, Selective laser melting of CoCrFeNiMn high entropy alloy powder modified with nano-TiN particles for additive manufacturing and strength enhancement: process, particle behavior and effects, Powder Technol 360 (2020) 509–521.
[114] Y.-K. Kim, M.-S. Baek, S. Yang, K.-A. Lee, In-situ formed oxide enables extraordinary high-cycle fatigue resistance in additively manufactured CoCrFeMnNi high-entropy alloy, Addit. Manuf. 38 (2021) 101832.
[115] Y. Kuzminova, A. Shibalova, S. Evlashin, I. Shishkovsky, P. Krakhmalev, Structural effect of low Al content in the in-situ additive manufactured CrFeCoNiAlx high-entropy alloy, Mater. Lett. 303 (2021) 130487.
[116] P. Chen, S. Li, Y. Zhou, M. Yan, M.M. Attallah, Fabricating CoCrFeMnNi high entropy alloy via selective laser melting in-situ alloying, J. Mater. Sci. Technol. 43 (2020) 40–43.
[117] J. Liu, J. Li, X. Du, Y. Tong, R. Wang, D. He, Z. Cai, H. Wang, Microstructure and mechanical properties of wire arc additively manufactured MoNbTaWTi high entropy alloys, Materials 14 (16) (2021).
[118] A. Zavdoveev, A. Klapatyuk, T. Baudin, E. MacDonald, D. Mohan, J.P. Oliveira, A. Gajvoronskiy, V. Poznyakov, H.S. Kim, F. Brisset, M. Khokhlov, M. Heaton, M. Rogante, M. Skoryk, D. Vedel, R. Kozin, I. Klochkov, S. Motrunich, Non-equimolar Cantor high entropy alloy fabrication using metal powder cored wire arc additive manufacturing, Additive Manufacturing Letters 6 (2023) 100124.
[119] B. Shi, D. Xin, X. Chen, Y. Wang, A. Singh, Fabrication of high-strength dual FCC phase Co-Cr-Fe-Ni-Cu-Mo high entropy alloy by plasma arc additive manufacturing using a combined cable wire, Mater. Lett. 337 (2023) 133983.
[120] T.A. Rodrigues, N. Bairrão, F.W.C. Farias, A. Shamsolhodaei, J. Shen, N. Zhou, E. Maawad, N. Schell, T.G. Santos, J.P. Oliveira, Steel-copper functionally graded material produced by twin-wire and arc additive manufacturing (T-WAAM), Mater. Des. 213 (2022) 110270.
[121] G. Bi, Y. Chew, F. Weng, Z. Zhu, F.L. Ng, B.Y. Lee, Process Study and Characterization of Properties of FerCrNiMnCo High-Entropy Alloys Fabricated by Laser-Aided Additive Manufacturing, SPIE, 2018.
[122] R. Li, P. Niu, T. Yuan, P. Cao, C. Chen, K. Zhou, Selective laser melting of an equiatomic CoCrFeMnNi high-entropy alloy: processability, non-equilibrium microstructure and mechanical property, J. Alloys Compd. 746 (2018) 125–134.
[123] S. Luo, P. Gao, H. Yu, J. Yang, Z. Wang, X. Zeng, Selective laser melting of an equiatomic AlCrCuFeNi high-entropy alloy: processability, non-equilibrium microstructure and mechanical behavior, J. Alloys Compd. 771 (2019) 387–397.
[124] P. Agrawal, R.S. Haridas, S. Thapliyal, S. Yadav, R.S. Mishra, B.A. McWilliams, K. C. Cho, Metastable high entropy alloys: an excellent defect tolerant material for additive manufacturing, Mater. Sci. Eng., A 826 (2021) 142005.
[125] I. Gibson, D. Rosen, B. Stucker, Additive manufacturing technologies: 3D printing, in: Rapid Prototyping, and Direct Digital Manufacturing 2nd, Springer New York, New York, NY, 2015, p. 2015.
[126] L. Guo, J. Gu, B. Gan, S. Ni, Z. Bi, Z. Wang, M. Song, Effects of elemental segregation and scanning strategy on the mechanical properties and hot cracking of a selective laser melted FeCoCrNiMn-(N,Si) high entropy alloy, J. Alloys Compd. 865 (2021) 158892.
[127] W. Zhang, H. Wang, B.J. Kooi, Y. Pei, Additive manufacturing of interstitial-strengthened high entropy alloy: scanning strategy dependent anisotropic mechanical properties, Mater. Sci. Eng., A 872 (2023) 144978.
[128] Q. Li, X.-R. Li, B.-X. Dong, X.-L. Zhang, S.-L. Shu, F. Qiu, L.-C. Zhang, Z.-H. Zhang, Metallurgy and solidification microstructure control of fusion-based additive manufacturing fabricated metallic alloys: a review, Acta Metall. Sin. 37 (1) (2024) 29–53.
[129] L. Zhou, H. Hyer, S. Thapliyal, R.S. Mishra, B. McWilliams, K. Cho, Y. Sohn, Process-dependent composition, microstructure, and printability of Al-Zn-Mg and Al-Zn-Mg-Sc-Zr alloys manufactured by laser powder bed fusion, Metall. Mater. Trans. 51 (6) (2020) 3215–3227.
[130] Y. Ekubaru, O. Gokcekaya, T. Ishimoto, K. Sato, K. Manabe, P. Wang, T. Nakano, Excellent strength–ductility balance of Sc-Zr-modified Al–Mg alloy by tuning bimodal microstructure via hatch spacing in laser powder bed fusion, Mater. Des. 221 (2022) 110976.
[131] P.V. Cobbinah, S. Matsunaga, Y. Toda, R. Ozasa, M. Okugawa, T. Ishimoto, Y. Liu, Y. Koizumi, P. Wang, T. Nakano, Y. Yamabe-Mitarai, Peculiar microstructural evolution and hardness variation depending on laser powder bed fusion-manufacturing condition in Ti–6Al–2Sn–4Zr–6Mo. Smart Materials in Manufacturing 2, 2024.
[132] H. Shiratori, T. Fujieda, K. Yamanaka, Y. Koizumi, K. Kuwabara, T. Kato, A. Chiba, Relationship between the microstructure and mechanical properties of an equiatomic AlCoCrFeNi high-entropy alloy fabricated by selective electron beam melting, Mater. Sci. Eng., A 656 (2016) 39–46.
[133] K. Kuwabara, H. Shiratori, T. Fujieda, K. Yamanaka, Y. Koizumi, A. Chiba, Mechanical and corrosion properties of AlCoCrFeNi high-entropy alloy fabricated with selective electron beam melting, Addit. Manuf. 23 (2018) 264–271.
[134] M. Joele, W.R. Matizamhuka, A review on the high temperature strengthening mechanisms of high entropy superalloys (HESA), Materials 14 (19) (2021).
[135] F. Wei, S. Wei, K.B. Lau, W.H. Teh, J.J. Lee, H.L. Seng, C.C. Tan, P. Wang, U. Ramamurty, Compositionally graded AlxCoCrFeNi high-entropy alloy manufactured by laser powder bed fusion, Materialia 21 (2022) 101308.
[136] M. Zhang, J. Li, Y. Li, J. Wang, Z. Li, X. Cheng, Effect of Al addition on the microstructure and hardness of the (AlxCoCrFe)50Ni high-entropy alloy prepared by directed energy deposition technique, Mater. Lett. 285 (2021) 128778.
[137] Z.U. Arif, M.Y. Khalid, A. Al Rashid, E. ur Rehman, M. Atif, Laser deposition of high-entropy alloys: a comprehensive review, Opt Laser. Technol. 145 (2022) 107447.
[138] P. Wang, X. Tan, C. He, M.L.S. Nai, R. Huang, S.B. Tor, J. Wei, Scanning optical microscopy for porosity quantification of additively manufactured components, Addit. Manuf. 21 (2018) 350–358.
[139] S. Huang, R.L. Narayan, J.H.K. Tan, S.L. Sing, W.Y. Yeong, Resolving the porosity-unmelted inclusion dilemma during in-situ alloying of Ti34Nb via laser powder bed fusion, Acta Mater. 204 (2021) 116522.
[140] P. Wang, M.H. Goh, Q. Li, M.L.S. Nai, J. Wei, Effect of defects and specimen size with rectangular cross-section on the tensile properties of additively manufactured components, Virtual Phys. Prototyp. 15 (3) (2020) 251–264.
[141] B. Li, L. Zhang, Y. Xu, Z. Liu, B. Qian, F. Xuan, Selective laser melting of CoCrFeNiMn high entropy alloy powder modified with nano-TiN particles for additive manufacturing and strength enhancement: process, particle behavior and effects, Powder Technol. 360 (2020) 509–521.
[142] P. Ferro, R. Meneghello, G. Savio, F. Berto, A modified volumetric energy density–based approach for porosity assessment in additive manufacturing process design, Int. J. Adv. Des. Manuf. Technol. 110 (7) (2020) 1911–1921.
[143] P.C. Collins, D.A. Brice, P. Samimi, I. Ghamarian, H.L. Fraser, Microstructural control of additively manufactured metallic materials, Annu. Rev. Mater. Res. 46 (1) (2016) 63–91.
[144] S. Cao, H. Wang, X. Lu, J. Tong, Z. Sheng, Topology optimization considering porosity defects in metal additive manufacturing, Appl. Sci. 11 (12) (2021) 5578.

[145] D. Wang, J. Lu, S. Tang, L. Yu, H. Fan, L. Ji, C. Liu, Reducing porosity and refining grains for arc additive manufacturing aluminum alloy by adjusting arc pulse frequency and current, Materials 11 (8) (2018) 1344.
[146] C. Li, M. Ferry, J.J. Kruzic, X. Li, Review: multi-principal element alloys by additive manufacturing, J. Mater. Sci. 57 (21) (2022) 9903–9935.
[147] L.R. Owen, N.G. Jones, Lattice distortions in high-entropy alloys, J. Mater. Res. 33 (19) (2018) 2954–2969.
[148] S.S. Nene, Some distinct features of transformative high entropy alloys for metal additive manufacturing, Front. Mater. 9 (2022).
[149] Z. Sun, X. Tan, C. Wang, M. Descoins, D. Mangelinck, S.B. Tor, E.A. Jägle, S. Zaefferer, D. Raabe, Reducing hot tearing by grain boundary segregation engineering in additive manufacturing: example of an AlxCoCrFeNi high-entropy alloy, Acta Mater. 204 (2021) 116505.
[150] S. Thapliyal, P. Agrawal, P. Agrawal, S.S. Nene, R.S. Mishra, B.A. McWilliams, K. C. Cho, Segregation engineering of grain boundaries of a metastable Fe-Mn-Co-Cr-Si high entropy alloy with laser-powder bed fusion additive manufacturing, Acta Mater. 219 (2021) 117271.
[151] R.-d. Li, P.-d. Niu, T.-c. Yuan, Z.-m. Li, Displacive transformation as pathway to prevent micro-cracks induced by thermal stress in additively manufactured strong and ductile high-entropy alloys, Trans. Nonferrous Metals Soc. China 31 (4) (2021) 1059–1073.
[152] F. Yang, L. Wang, Z. Wang, Q. Wu, K. Zhou, X. Lin, W. Huang, Ultra strong and ductile eutectic high entropy alloy fabricated by selective laser melting, J. Mater. Sci. Technol. 106 (2022) 128–132.
[153] S. Gou, M. Gao, Y. Shi, S. Li, Y. Fang, X. Chen, H. Chen, W. Yin, J. Liu, Z. Lei, H. Wang, Additive manufacturing of ductile refractory high-entropy alloys via phase engineering, Acta Mater. 248 (2023) 118781.
[154] H. Huang, Y. Wu, J. He, H. Wang, X. Liu, K. An, W. Wu, Z. Lu, Phase-transformation ductilization of brittle high-entropy alloys via metastability engineering, Adv. Mater. 29 (30) (2017) 1701678.
[155] H. Yi, M. Bi, K. Yang, B. Zhang, Significant improvement the mechanical properties of CoCrNi alloy by tailoring a dual FCC-phase structure, Materials 13 (21) (2020) 4909.
[156] Y. Cai, M. Shan, Y. Cui, S.M. Manladan, X. Lv, L. Zhu, D. Sun, T. Wang, J. Han, Microstructure and properties of FeCoCrNi high entropy alloy produced by laser melting deposition, J. Alloys Compd. 887 (2021) 161323.
[157] T. Ishimoto, R. Ozasa, K. Nakano, M. Weinmann, C. Schnitter, M. Stenzel, A. Matsugaki, T. Nagase, T. Matsuzaka, M. Todai, H.S. Kim, T. Nakano, Development of TiNbTaZrMo bio-high entropy alloy (BioHEA) super-solid solution by selective laser melting, and its improved mechanical property and biocompatibility, Scripta Mater. 194 (2021) 113658.
[158] H. Chen, T. Lu, Y. Wang, Y. Liu, T. Shi, K.G. Prashanth, K. Kosiba, Laser additive manufacturing of nano-TiC particles reinforced CoCrFeMnNi high-entropy alloy matrix composites with high strength and ductility, Mater. Sci. Eng., A 833 (2022) 142512.
[159] H. Peng, S. Xie, P. Niu, Z. Zhang, T. Yuan, Z. Ren, X. Wang, Y. Zhao, R. Li, Additive manufacturing of Al0.3CoCrFeNi high-entropy alloy by powder feeding laser melting deposition, J. Alloys Compd. 862 (2021) 158286.
[160] Y.-T. Chen, Y.-J. Chang, H. Murakami, T. Sasaki, K. Hono, C.-W. Li, K. Kakehi, J.-W. Yeh, A.-C. Yeh, Hierarchical microstructure strengthening in a single crystal high entropy superalloy, Sci. Rep. 10 (1) (2020) 12163.
[161] S. Wang, Y. Li, D. Zhang, Y. Yang, S. Marwana Manladan, Z. Luo, Microstructure and mechanical properties of high strength AlCoCrFeNi2.1 eutectic high entropy alloy prepared by selective laser melting (SLM), Mater. Lett. 310 (2022) 131511.
[162] H. Li, Y. Huang, J. Sun, Y. Lu, The relationship between thermo-mechanical history, microstructure and mechanical properties in additively manufactured CoCrFeMnNi high entropy alloy, J. Mater. Sci. Technol. 77 (2021) 187–195.
[163] C. Kenel, N.P.M. Casati, D.C. Dunand, 3D ink-extrusion additive manufacturing of CoCrFeNi high-entropy alloy micro-lattices, Nat. Commun. 10 (1) (2019) 904.
[164] D. Lin, L. Xu, H. Jing, Y. Han, L. Zhao, F. Minami, Effects of annealing on the structure and mechanical properties of FeCoCrNi high-entropy alloy fabricated via selective laser melting, Addit. Manuf. 32 (2020) 101058.
[165] C. Haase, F. Tang, M.B. Wilms, A. Weisheit, B. Hallstedt, Combining thermodynamic modeling and 3D printing of elemental powder blends for high-throughput investigation of high-entropy alloys – towards rapid alloy screening and design, Mater. Sci. Eng., A 688 (2017) 180–189.
[166] N. Eißmann, B. Klöden, T. Weißgärber, B. Kieback, High-entropy alloy CoCrFeMnNi produced by powder metallurgy, Powder Metall. 60 (3) (2017) 184–197.
[167] S. Guan, D. Wan, K. Solberg, F. Berto, T. Welo, T.M. Yue, K.C. Chan, Additive manufacturing of fine-grained and dislocation-populated CrMnFeCoNi high entropy alloy by laser engineered net shaping, Mater. Sci. Eng., A 761 (2019) 138056.
[168] Y. Chew, G.J. Bi, Z.G. Zhu, F.L. Ng, F. Weng, S.B. Liu, S.M.L. Nai, B.Y. Lee, Microstructure and enhanced strength of laser aided additive manufactured CoCrFeNiMn high entropy alloy, Mater. Sci. Eng., A 744 (2019) 137–144.
[169] Z. Tong, X. Ren, J. Jiao, W. Zhou, Y. Ren, Y. Ye, E.A. Larson, J. Gu, Laser additive manufacturing of FeCrCoMnNi high-entropy alloy: effect of heat treatment on microstructure, residual stress and mechanical property, J. Alloys Compd. 785 (2019) 1144–1159.
[170] J. Joseph, P. Hodgson, T. Jarvis, X. Wu, N. Stanford, D.M. Fabijanic, Effect of hot isostatic pressing on the microstructure and mechanical properties of additive manufactured AlxCoCrFeNi high entropy alloys, Mater. Sci. Eng., A 733 (2018) 59–70.
[171] P.F. Zhou, D.H. Xiao, Z. Wu, X.Q. Ou, Al0.5FeCoCrNi high entropy alloy prepared by selective laser melting with gas-atomized pre-alloy powders, Mater. Sci. Eng., A 739 (2019) 86–89.
[172] R. Wang, K. Zhang, C. Davies, X. Wu, Evolution of microstructure, mechanical and corrosion properties of AlCoCrFeNi high-entropy alloy prepared by direct laser fabrication, J. Alloys Compd. 694 (2017) 971–981.
[173] W. Wu, R. Zhou, B. Wei, S. Ni, Y. Liu, M. Song, Nanosized precipitates and dislocation networks reinforced C-containing CoCrFeNi high-entropy alloy fabricated by selective laser melting, Mater. Char. 144 (2018) 605–610.
[174] H. Zhang, Y. Zhao, S. Huang, S. Zhu, F. Wang, D. Li, Manufacturing and analysis of high-performance refractory high-entropy alloy via selective laser melting (SLM), Materials 12 (5) (2019) 720.
[175] R. Zhou, Y. Liu, C. Zhou, S. Li, W. Wu, M. Song, B. Liu, X. Liang, P.K. Liaw, Microstructures and mechanical properties of C-containing FeCoCrNi high-entropy alloy fabricated by selective laser melting, Intermetallics 94 (2018) 165–171.
[176] R. Zhou, Y. Liu, B. Liu, J. Li, Q. Fang, Precipitation behavior of selective laser melted FeCoCrNiC0.05 high entropy alloy, Intermetallics 106 (2019) 20–25.
[177] J.M. Park, J. Choe, J.G. Kim, J.W. Bae, J. Moon, S. Yang, K.T. Kim, J.-H. Yu, H. S. Kim, Superior tensile properties of 1%C-CoCrFeMnNi high-entropy alloy additively manufactured by selective laser melting, Mater. Res. Lett. (2019) 1–7.
[178] M. Song, R. Zhou, J. Gu, Z. Wang, S. Ni, Y. Liu, Nitrogen induced heterogeneous structures overcome strength-ductility trade-off in an additively manufactured high-entropy alloy, Appl. Mater. Today 18 (2020) 100498.
[179] Z. Wang, J. Gu, D. An, Y. Liu, M. Song, Characterization of the microstructure and deformation substructure evolution in a hierarchal high-entropy alloy by correlative EBSD and ECCI, Intermetallics 121 (2020) 106788.
[180] R.J. Vikram, B.S. Murty, D. Fabijanic, S. Suwas, Insights into micro-mechanical response and texture of the additively manufactured eutectic high entropy alloy AlCoCrFeNi2.1, J. Alloys Compd. 827 (2020) 154034.
[181] Y. Wang, R. Li, P. Niu, Z. Zhang, T. Yuan, J. Yuan, K. Li, Microstructures and properties of equimolar AlCoCrCuFeNi high-entropy alloy additively manufactured by selective laser melting, Intermetallics 120 (2020) 106746.
[182] P.K. Sarswat, S. Sarkar, A. Murali, W. Huang, W. Tan, M.L. Free, Additive manufactured new hybrid high entropy alloys derived from the AlCoFeNiSmTiVZr system, Appl. Surf. Sci. 476 (2019) 242–258.
[183] Z. Cai, G. Jin, X. Cui, Z. Liu, W. Zheng, Y. Li, L. Wang, Synthesis and microstructure characterization of Ni-Cr-Co-Ti-V-Al high entropy alloy coating on Ti-6Al-4V substrate by laser surface alloying, Mater. Char. 120 (2016) 229–233.
[184] B. Li, B. Qian, Y. Xu, Z. Liu, F. Xuan, Fine-structured CoCrFeNiMn high-entropy alloy matrix composite with 12 wt% TiN particle reinforcements via selective laser melting assisted additive manufacturing, Mater. Lett. 252 (2019) 88–91.
[185] B. Li, L. Zhang, B. Yang, Grain refinement and localized amorphization of additively manufactured high-entropy alloy matrix composites reinforced by nano ceramic particles via selective-laser-melting/remelting, Compos. Commun. 19 (2020) 56–60.
[186] Y.L. Wang, L. Zhao, D. Wan, S. Guan, K.C. Chan, Additive manufacturing of TiB2-containing CoCrFeMnNi high-entropy alloy matrix composites with high density and enhanced mechanical properties, Mater. Sci. Eng., A 825 (2021) 141871.
[187] R. Savinov, Y. Wang, J. Shi, Microstructure and properties of CeO2-doped CoCrFeMnNi high entropy alloy fabricated by laser metal deposition, J. Manuf. Process. 56 (2020) 1245–1251.
[188] S. Guan, D. Wan, K. Solberg, F. Berto, T. Welo, T.M. Yue, K.C. Chan, Additively manufactured CrMnFeCoNi/AlCoCrFeNiTi0.5 laminated high-entropy alloy with enhanced strength-plasticity synergy, Scripta Mater. 183 (2020) 133–138.
[189] P.D. Niu, R.D. Li, T.C. Yuan, S.Y. Zhu, C. Chen, M.B. Wang, L. Huang, Microstructures and properties of an equimolar AlCoCrFeNi high entropy alloy printed by selective laser melting, Intermetallics 104 (2019) 24–32.
[190] Y.O. Kuzminova, D.G. Firsov, S.A. Dagesyan, S.D. Konev, S.N. Sergeev, A. P. Zhilyaev, M. Kawasaki, I.S. Akhatov, S.A. Evlashin, Fatigue behavior of additive manufactured CrFeCoNi medium-entropy alloy, J. Alloys Compd. 863 (2021) 158609.
[191] Y. Chen, B. Li, B. Chen, F. Xuan, High-cycle fatigue induced twinning in CoCrFeNi high-entropy alloy processed by laser powder bed fusion additive manufacturing, Addit. Manuf. 61 (2023) 103319.
[192] A. Piglione, B. Dovgyy, C. Liu, C.M. Gourlay, P.A. Hooper, M.S. Pham, Printability and microstructure of the CoCrFeMnNi high-entropy alloy fabricated by laser powder bed fusion, Mater. Lett. 224 (2018) 22–25.
[193] J. Wang, M. Zhang, H. Wang, Z. Li, X. Cheng, B. Zhang, J. Li, X. Ran, Mitigating hot-cracking of laser melted CoCrFeNiMnTix high-entropy alloys, Mater. Lett. 314 (2022) 131771.
[194] H.R. Sistla, J.W. Newkirk, F. Frank Liou, Effect of Al/Ni ratio, heat treatment on phase transformations and microstructure of AlxFeCoCrNi2−x (x=0.3, 1) high entropy alloys, Mater. Des. 81 (2015) 113–121.
[195] B. Gwalani, S. Gangireddy, S. Shukla, C.J. Yannetta, S.G. Valentin, R.S. Mishra, R. Banerjee, Compositionally graded high entropy alloy with a strong front and ductile back, Mater. Today Commun. 20 (2019) 100602.
[196] C.-W. Li, K.-C. Chang, A.-C. Yeh, On the microstructure and properties of an advanced cemented carbide system processed by selective laser melting, J. Alloys Compd. 782 (2019) 440–450.
[197] B. Su, J. Li, C. Yang, Y. Zhang, Z. Li, Y. Zhang, Microstructure and mechanical properties of a refractory AlMo0.5NbTa0.5TiZr high-entropy alloy manufactured by laser-directed energy deposition, Mater. Lett. 335 (2023) 133748.
[198] F. Wang, Y. Guo, Q. Liu, X. Shang, A novel D022 precipitation-hardened Ni2.1CoCrFe0.5Nb0.2 high entropy alloy with outstanding tensile properties by additive manufacturing, Virtual Phys. Prototyp. 18 (1) (2023) e2147553.

[199] K. Yuan, X. Yao, Y. Yu, R. Wang, Z. Chai, K. Zhou, Z. Wang, Dynamic thermomechanical response and constitutive modeling of eutectic high-entropy alloy, Int. J. Mech. Sci. 246 (2023) 108148.
[200] H. Zhang, J. Cai, J. Geng, X. Sun, Y. Zhao, X. Guo, D. Li, Study on annealing treatment of NbMoTaTiNi high-entropy alloy with ultra-high strength disordered-ordered transition structure for additive manufacturing, J. Alloys Compd. 941 (2023) 168810.
[201] H. Dobbelstein, E.L. Gurevich, E.P. George, A. Ostendorf, G. Laplanche, Laser metal deposition of compositionally graded TiZrNbTa refractory high-entropy alloys using elemental powder blends, Addit. Manuf. 25 (2019) 252–262.
[202] B. Xiao, H. Liu, W. Jia, J. Wang, L. Zhou, Cracking suppression in selective electron beam melted WMoTaNbC refractory high-entropy alloy, J. Alloys Compd. 948 (2023) 169787.
[203] O.N. Senkov, G.B. Wilks, J.M. Scott, D.B. Miracle, Mechanical properties of Nb25Mo25Ta25W25 and V20Nb20Mo20Ta20W20 refractory high entropy alloys, Intermetallics 19 (5) (2011) 698–706.
[204] H.G. Li, T.L. Lee, W. Zheng, Y.Z. Lu, H.B.C. Yin, J.X. Yang, Y.J. Huang, J.F. Sun, Characterization of residual stress in laser melting deposited CoCrFeMnNi high entropy alloy by neutron diffraction, Mater. Lett. 263 (2020) 127247.
[205] J. Ren, Y. Zhang, D. Zhao, Y. Chen, S. Guan, Y. Liu, L. Liu, S. Peng, F. Kong, J. D. Poplawsky, G. Gao, T. Voisin, K. An, Y.M. Wang, K.Y. Xie, T. Zhu, W. Chen, Strong yet ductile nanolamellar high-entropy alloys by additive manufacturing, Nature 608 (7921) (2022) 62–68.
[206] S. Xiang, H. Luan, J. Wu, K.-F. Yao, J. Li, X. Liu, Y. Tian, W. Mao, H. Bai, G. Le, Q. Li, Microstructures and mechanical properties of CrMnFeCoNi high entropy alloys fabricated using laser metal deposition technique, J. Alloys Compd. 773 (2019) 387–392.
[207] J. Li, H. Luan, L. Zhou, A. Amar, R. Li, L. Huang, X. Liu, G. Le, X. Wang, J. Wu, C. Jiang, Phase transformation - induced strengthening of an additively manufactured multi- principal element CrMnFeCoNi alloy, Mater. Des. 195 (2020) 108999.
[208] Y.-K. Kim, M.-C. Kim, K.-A. Lee, 1.45 GPa ultrastrong cryogenic strength with superior impact toughness in the in-situ nano oxide reinforced CrMnFeCoNi high-entropy alloy matrix nanocomposite manufactured by laser powder bed fusion, J. Mater. Sci. Technol. 97 (2022) 10–19.
[209] Y. Kuzminova, D. Firsov, A. Dudin, S. Sergeev, A. Zhilyaev, A. Dyakov, A. Chupeeva, A. Alekseev, D. Martynov, I. Akhatov, S. Evlashin, The effect of the parameters of the powder bed fusion process on the microstructure and mechanical properties of CrFeCoNi medium-entropy alloys, Intermetallics 116 (2020) 106651.
[210] T.M. Smith, C.A. Kantzos, N.A. Zarkevich, B.J. Harder, M. Heczko, P.R. Gradl, A. C. Thompson, M.J. Mills, T.P. Gabb, J.W. Lawson, A 3D printable alloy designed for extreme environments, Nature 617 (2023) 513–518.
[211] J. Li, S. Xiang, H. Luan, A. Amar, X. Liu, S. Lu, Y. Zeng, G. Le, X. Wang, F. Qu, C. Jiang, G. Yang, Additive manufacturing of high-strength CrMnFeCoNi high-entropy alloys-based composites with WC addition, J. Mater. Sci. Technol. 35 (11) (2019) 2430–2434.
[212] H.-I. Jeong, C.-M. Lee, D.-H. Kim, Manufacturing of Ti–Nb–Cr–V–Ni high entropy alloy using directed energy deposition and evaluation of materials properties, J. Mater. Res. Technol. 23 (2023) 5606–5617.
[213] P. Niu, R. Li, S. Zhu, M. Wang, C. Chen, T. Yuan, Hot cracking, crystal orientation and compressive strength of an equimolar CoCrFeMnNi high-entropy alloy printed by selective laser melting, Opt Laser. Technol. 127 (2020) 106147.
[214] Y.-K. Kim, J. Choe, K.-A. Lee, Selective laser melted equiatomic CoCrFeMnNi high-entropy alloy: microstructure, anisotropic mechanical response, and multiple strengthening mechanism, J. Alloys Compd. 805 (2019) 680–691.
[215] Q. Li, H. Zhang, D. Li, Z. Chen, S. Huang, Z. Lu, H. Yan, WxNbMoTa refractory high-entropy alloys fabricated by laser cladding deposition, Materials 12 (3) (2019) 533.
[216] Y. Qiu, M.A. Gibson, H.L. Fraser, N. Birbilis, Corrosion characteristics of high entropy alloys, Mater. Sci. Technol. 31 (10) (2015) 1235–1243.
[217] Y. Qiu, S. Thomas, M.A. Gibson, H.L. Fraser, N. Birbilis, Corrosion of high entropy alloys, npj Mater. Degrad. 1 (1) (2017) 15.
[218] Y.Y. Chen, T. Duval, U.D. Hung, J.W. Yeh, H.C. Shih, Microstructure and electrochemical properties of high entropy alloys—a comparison with type-304 stainless steel, Corrosion Sci. 47 (9) (2005) 2257–2279.
[219] Y.-J. Hsu, W.-C. Chiang, J.-K. Wu, Corrosion behavior of FeCoNiCrCux high-entropy alloys in 3.5% sodium chloride solution, Mater. Chem. Phys. 92 (1) (2005) 112–117.
[220] C.-W. Tsai, M.-H. Tsai, J.-W. Yeh, C.-C. Yang, Effect of temperature on mechanical properties of Al0.5CoCrCuFeNi wrought alloy, J. Alloys Compd. 490 (1) (2010) 160–165.
[221] J. Ren, C. Mahajan, L. Liu, D. Follette, W. Chen, S. Mukherjee, Corrosion behavior of selectively laser melted CoCrFeMnNi high entropy alloy, Metals 9 (10) (2019).
[222] M. Dada, P. Popoola, N. Mathe, S. Pityana, S. Adeosun, O. Aramide, The comparative study of the microstructural and corrosion behaviour of laser-deposited high entropy alloys, J. Alloys Compd. 866 (2021) 158777.
[223] R. Zhou, W. Chen, W. Li, T.-H. Chou, Y.-H. Chen, X. Liang, J. Luan, Y. Zhu, J. C. Huang, Y. Liu, 3D printed N-doped CoCrFeNi high entropy alloy with more than doubled corrosion resistance in dilute sulphuric acid, npj Mater. Degrad. 7 (1) (2023) 8.
[224] Q. Wang, A. Amar, C. Jiang, H. Luan, S. Zhao, H. Zhang, G. Le, X. Liu, X. Wang, X. Yang, J. Li, CoCrFeNiMo0.2 high entropy alloy by laser melting deposition: prospective material for low temperature and corrosion resistant applications, Intermetallics 119 (2020) 106727.
[225] A. Amiri, R. Shahbazian-Yassar, Recent progress of high-entropy materials for energy storage and conversion, J. Mater. Chem. A 9 (2) (2021) 782–823.
[226] J.W. Sturman, E.A. Baranova, Y. Abu-Lebdeh, Review: high-entropy materials for lithium-ion battery electrodes, Front. Energy Res. 10 (2022).
[227] F. Marques, M. Balcerzak, F. Winkelmann, G. Zepon, M. Felderhoff, Review and outlook on high-entropy alloys for hydrogen storage, Energy Environ. Sci. 14 (10) (2021) 5191–5227.
[228] J. Feng, Y. Tang, J. Liu, P. Zhang, C. Liu, L. Wang, Bio-high entropy alloys: progress, challenges, and opportunities, Front. Bioeng. Biotechnol. 10 (2022).
[229] G. Ren, L. Huang, K. Hu, T. Li, Y. Lu, D. Qiao, H. Zhang, D. Xu, T. Wang, T. Li, P. K. Liaw, Enhanced antibacterial behavior of a novel Cu-bearing high-entropy alloy, J. Mater. Sci. Technol. 117 (2022) 158–166.
[230] C. Chen, J. Chen, S. Yuan, W. Li, W. Wang, X. Li, W. Zhang, R. Wei, S. Guan, T. Wang, T. Zhang, N. Lei, F. Li, Microstructure, mechanical properties, corrosion resistance and anti-bacterial behavior of novel Co-free high entropy alloys, J. Alloys Compd. 902 (2022) 163714.
[231] P. Kumar, N.K. Jain, S. Jaiswal, S. Gupta, Development of Ti–Ta–Nb–Mo–Zr high entropy alloy by μ-plasma arc additive manufacturing process for knee implant applications and its biocompatibility evaluation, J. Mater. Res. Technol. 22 (2023) 541–555.
[232] J. Feng, D. Wei, P. Zhang, Z. Yu, C. Liu, W. Lu, K. Wang, H. Yan, L. Zhang, L. Wang, Preparation of TiNbTaZrMo high-entropy alloy with tunable Young's modulus by selective laser melting, J. Manuf. Process. 85 (2023) 160–165.
[233] O. Gokcekaya, T. Ishimoto, Y. Nishikawa, Y.S. Kim, A. Matsugaki, R. Ozasa, M. Weinmann, C. Schnitter, M. Stenzel, H.S. Kim, Y. Miyabayashi, T. Nakano, Novel single crystalline-like non-equiatomic TiZrHfNbTaMo bio-high entropy alloy (BioHEA) developed by laser powder bed fusion, Mater. Res. Lett. 11 (4) (2023) 274–280.
[234] K.-H. Jung, M.T. Tran, Z. Shan, H.W. Lee, S.-K. Hwang, H.G. Kim, D.-K. Kim, Correlation of cryogenic deformation mechanisms to excellent strength-ductility of CrCoNi medium entropy alloy processed by selective laser melting, J. Mater. Res. Technol. 22 (2023) 2297–2315.
[235] D. Liu, Q. Yu, S. Kabra, M. Jiang, P. Forna-Kreutzer, R. Zhang, M. Payne, F. Walsh, B. Gludovatz, M. Asta, A.M. Minor, E.P. George, R.O. Ritchie, Exceptional fracture toughness of CrCoNi-based medium- and high-entropy alloys at 20 kelvin, Science 378 (6623) (2022) 978–983.
[236] Y. Tong, D. Chen, B. Han, J. Wang, R. Feng, T. Yang, C. Zhao, Y.L. Zhao, W. Guo, Y. Shimizu, C.T. Liu, P.K. Liaw, K. Inoue, Y. Nagai, A. Hu, J.J. Kai, Outstanding tensile properties of a precipitation-strengthened FeCoNiCrTi0.2 high-entropy alloy at room and cryogenic temperatures, Acta Mater. 165 (2019) 228–240.
[237] P. Sathiyamoorthi, J. Moon, J.W. Bae, P. Asghari-Rad, H.S. Kim, Superior cryogenic tensile properties of ultrafine-grained CoCrNi medium-entropy alloy produced by high-pressure torsion and annealing, Scripta Mater. 163 (2019) 152–156.
[238] B. Gludovatz, A. Hohenwarter, K.V.S. Thurston, H. Bei, Z. Wu, E.P. George, R. O. Ritchie, Exceptional damage-tolerance of a medium-entropy alloy CrCoNi at cryogenic temperatures, Nat. Commun. 7 (2016) 10602.
[239] P. Kumar, M. Michalek, D.H. Cook, H. Sheng, K.B. Lau, P. Wang, M. Zhang, A. M. Minor, U. Ramamurty, R.O. Ritchie, On the strength and fracture toughness of an additive manufactured CrCoNi medium-entropy alloy, Acta Mater. 258 (2023) 119249.
[240] B. Han, C. Zhang, K. Feng, Z. Li, X. Zhang, Y. Shen, X. Wang, H. Kokawa, R. Li, Z. Wang, P.K. Chu, Additively manufactured high strength and ductility CrCoNi medium entropy alloy with hierarchical microstructure, Mater. Sci. Eng., A 820 (2021) 141545.
[241] F. Weng, Y. Chew, Z. Zhu, X. Yao, L. Wang, F.L. Ng, S. Liu, G. Bi, Excellent combination of strength and ductility of CoCrNi medium entropy alloy fabricated by laser aided additive manufacturing, Addit. Manuf. 34 (2020) 101202.
[242] H. Hadraba, Z. Chlup, A. Dlouhy, F. Dobes, P. Roupcova, M. Vilemova, J. Matejicek, Oxide dispersion strengthened CoCrFeNiMn high-entropy alloy, Mater. Sci. Eng., A 689 (2017) 252–256.
[243] M. Moschetti, P.A. Burr, E. Obbard, J.J. Kruzic, P. Hosemann, B. Gludovatz, Design considerations for high entropy alloys in advanced nuclear applications, J. Nucl. Mater. 567 (2022) 153814.
[244] Y. Zong, N. Hashimoto, H. Oka, Study on irradiation effects of refractory bcc high-entropy alloy, Nuclear Materials and Energy 31 (2022) 101158.
[245] O. El Atwani, H.T. Vo, M.A. Tunes, C. Lee, A. Alvarado, N. Krienke, J. D. Poplawsky, A.A. Kohnert, J. Gigax, W.Y. Chen, M. Li, Y.Q. Wang, J.S. Wróbel, D. Nguyen-Manh, J.K.S. Baldwin, O.U. Tukac, E. Aydogan, S. Fensin, E. Martinez, A quinary WTaCrVHf nanocrystalline refractory high-entropy alloy withholding extreme irradiation environments, Nat. Commun. 14 (1) (2023) 2516.
[246] P. Wang, X. Tan, M.L.S. Nai, S.B. Tor, J. Wei, Spatial and geometrical-based characterization of microstructure and microhardness for an electron beam melted Ti–6Al–4V component, Mater. Des. 95 (2016) 287–295.
[247] P. Wang, J. Song, M.L.S. Nai, J. Wei, Experimental analysis of additively manufactured component and design guidelines for lightweight structures: a case study using electron beam melting, Addit. Manuf. 33 (2020) 101088.
[248] X. Li, P. Wang, M. Zhao, X. Su, Y.H. Tan, J. Ding, Customizable anisotropic microlattices for additive manufacturing: machine learning accelerated design, mechanical properties and structural-property relationships, Addit. Manuf. 89 (2024) 104248.
[249] M. Cagirici, M.L.S. Nai, J. Wei, J. Ding, P. Wang, Effect of annealing conditions on microstructure and hardness of CoCrFeNiMn-0.18Ti high entropy alloy manufactured by electron beam melting, J. Additive Manufacturing Technol. 1 (2) (2021) 526.

[250] B.Q. Li, L. Wang, B.B. Wang, D.H. Li, J.P. Oliveira, R. Cui, J.X. Yu, L.S. Luo, R. R. Chen, Y.Q. Su, J.J. Guo, H.Z. Fu, Tuning the microstructure, martensitic transformation and superelastic properties of EBF3-fabricated NiTi shape memory alloy using interlayer remelting, Mater. Des. 220 (2022).
[251] Y.K. Kim, S. Yang, K.A. Lee, Superior temperature-dependent mechanical properties and deformation behavior of equiatomic CoCrFeMnNi high-entropy alloy additively manufactured by selective laser melting, Sci. Rep. 10 (1) (2020) 8045.
[252] Z.G. Zhu, X.H. An, W.J. Lu, Z.M. Li, F.L. Ng, X.Z. Liao, U. Ramamurty, S.M.L. Nai, J. Wei, Selective laser melting enabling the hierarchically heterogeneous microstructure and excellent mechanical properties in an interstitial solute strengthened high entropy alloy, Mater. Res. Lett. 7 (11) (2019) 453–459.